The Pennsylvania State University

The Graduate School

Department of Energy and Mineral Engineering

MICRO-HOLLOW CATHODE DISCHARGE ANALYSIS OF LUNAR REGOLITH SIMULANTS

A Thesis in

Energy & Mineral Engineering

by

Amrita Mukherjee

Submitted in Partial Fulfillment

of the Requirements

for the Degree of

Master of Science

May 2012

The thesis of Amrita Mukherjee was reviewed and approved* by the following:

Randy L. Vander Wal

Associate Professor of Energy and Mineral Engineering,

Material Science and Engineering and Mechanical Engineering

Thesis Adviser

Miriam Freedman

Assistant Professor of Chemistry

Robert Larry Grayson

Professor of Energy and Mineral Engineering

Graduate Program Officer of Energy and Mineral Engineering

Yaw D. Yeboah

Professor and Department Head of Energy and Mineral Engineering

*Signatures are on file in the Graduate School

ABSTRACT

The main objective of this work was to develop and demonstrate a Micro-Hollow Cathode Discharge (MHCD) method for the compositional analysis of lunar regolith simulants. The MHCD technique thus developed was tested for the basic analytical figures of merit such as elemental detection and concentration, linearity and dynamic range and sensitivity to matrix effects. Analytical precision and accuracy, the two key factors, essential for analytical analysis were also evaluated.

The data from the MHCD are presented in two formats. The first is in the form of scaling factors that include both instrumental response and proportionality of signal to element concentration within a particular mineral. This data is presented in the format of separate plots of scaling factors for each element, across the simulants. By this cross-simulant comparison, variations in element sensitivity, i.e. signal per unit concentration, is viewed across the range of simulants tested. This affords direct testing of potential matrix effects. Such effects may arise because of different crystallography or bonding of the elements of interest within the different mineral components of the simulants. If manifested, depending upon their magnitude, it may present limitations on accuracy of elemental concentrations or more broadly limit the ability to identify minerals based upon their elemental concentrations.

The second method of comparing the datasets from the simulants was by element concentration, as varied by simulant identity. This comparison was aligned with standard analytical evaluation for signal linearity and dynamic range. In this study the limits for

each metric were set by the range of simulants and their corresponding mineral contents. Apart from this fundamental analytical evaluation, a key reason for this evaluation was to illustrate the manner by which a sample of unknown mineral content would be compared to a database of known minerals for a particular experimental configuration of the MHCD-OES (Micro-Hollow Cathode Discharge Optical Emission Spectroscopy) technique. Though the MHCD signal is the dependent variable, signal from an unknown sample could be inverted through the calibration curve to determine an elemental concentration, for each element. The set of elemental concentrations so determined would then permit mineral identification.

Normalization of spectra accounts for signal variation with sample mass and change in intensity with time for any particular sample charge. To be noted, both of such data comparisons include instrumental response factors that vary with wavelength, and hence element identity. Therein as a mineral identification tool, the database and analyses would be specific to the instrumental configuration at this stage of development.

TABLE OF CONTENTS

LIST OF TABLES

ACKNOWLEDGEMENTS

I would like to express my profound gratitude to my adviser Dr. Randy VanderWal whose overwhelming help, support and guidance were present throughout my graduate studies. His exceptional lectures on plasma physics and engineering helped me gain better understanding of the subjects. I also want to thank Dr. Jane Hitomi Fujiyama Novak for her constant guidance and help during the first year of my Graduate life.

I extend my gratitude to Dr. Robert Larry Grayson and Dr. Miriam Freedman for serving on my committee and for their valuable feedback. I am thankful to Dr. Douglas Rickman, Project Scientist on NASA's Simulant Development Program at the Marshall Space Flight Center., for not only providing me with all the necessary samples (lunar simulants) but also for sharing with me valuable information about the Lunar Simulants. I am also very much grateful to my research group members Chethan Kumar Gaddam and Ganesh Rahul Bhimanapati for their help. Finally, I address special thanks to all my family, friends and colleagues. Their support has been a constant source of motivation for me during the past two years.

Finally, I would like to dedicate my M.S. thesis to my father Dr. Prabir Mukhopadhyay and my mother Mrs. Shikha Mukhopadhyay whose support and guidance helped me to move forward and achieve my goal.

Chapter 1

INTRODUCTION

This chapter provides an overview of the work done in this research and explains the motivations for such work.

Chapter Outline:

1.1 Motivation

1.2 Thesis Outline

1.1 Motivation

Plasmas are used as direct analytical tools for optical emission spectroscopy. Inductively coupled plasma (ICP)[1] and direct-current plasma (DCP)[2] instruments create high-temperature plasmas that perform the dual analytical function of atomizing and electronically exciting the constituent elements whose spectra uniquely identify the material composition. Glow discharge plasmas are also used in commercial laboratory instruments for atomization of solid samples. Typically a kW supply powers the glow discharge under a low-pressure inert gas to atomize near-surface layers of a material for subsequent mass spectrometric analysis[3]. Nevertheless, mass spectrometry is difficult to calibrate, particularly over a wide range of atomic masses.

In recent years the Micro-Hollow Cathode Discharge (MHCD) method has been miniaturized, thereby testing physical scaling relationships[4]. Specifically these relate the operating pressure to the relevant (hollow cathode) physical dimension, i.e., the

''hollow'' diameter[4]. Following White's relation[5], atmospheric pressure operation could be achieved with hollow cathode spatial dimensions on the order of 100μm diameter. Significantly the need for low-pressure operation and vacuum hardware is negated[6]. A second advantage is the drastic reduction of operating power. Both factors greatly simplify the supporting hardware[7]. Single and arrayed elements have been successfully demonstrated[8]. Todate, research on such microdischarges has focused primarily upon their applications to photonics and their use as VUV light sources [9]. Little work has been done using the MHCD for analytical purposes. Against this background, this research attempts to investigate the analytical utility of a MHCD device. Using recent advancements in MHCD technology for operation at atmospheric pressure, the traditional sputtering action of the glow plasma can be utilized to both atomize and electronically excite samples for stand-alone analytical analysis, akin to dedicated laboratory-scale instruments but now on a micro-scale with Watt-level power usage.

In this work MHCD was developed into an analytical device for the analysis of lunar regolith simulants. Presently the NASA Mars Science Laboratory (MSL) on the MARs Flagship mission scheduled for 2011 incorporates a LIBS instrument for rock and soil analysis[10]. This is to be supported on a large rover. LIBS produces a high-temperature, high-energy microplasma to vaporize and electronically excite the constituent elements. This high energy, often supra-thermal plasma produces an extremely bright spectral background through inverse Brehmstralung radiation[11]. Elemental detection is achieved by a temporal delay to allow the hot microplasma to cool. This operationally-defined delay and potential for sample matrix effects introduces considerable analysis complexity

in establishing concentrations and potentially limits analysis quantification in field applications. Moreover, the LIBS signal is sensitive to ambient gas (if present), its composition, pressure, plus spatial and spectral non-uniformities in the ablation plume, which are always present and temporally evolving.

In contrast to LIBS, the MHCD, as characteristic of glow-discharge plasmas, is a low-temperature, low-energy "cool" plasma (< 1000 K) for which there is no ultra-bright background radiation. Atomization is achieved by sputtering for solid samples. Operated as a steady-state analysis upon solid materials, the MHCD instrument potentially offers lower detection limits with high precision and accuracy. For planetary exploration, the MHCD has the potential to replace LIBS, by being a low-power, yet sensitive and accurate instrument.

Compared to other methods such as neutron or proton-induced X-ray emission (PIXIE)[12] or the alpha proton X-ray spectrometer (APXS) as used in the Mars Pathfinder Mission[13], the MHCD does not require sophisticated sources or detectors and it can efficiently detect all elements (so-called light, e.g. H and heavy, e.g. transition metals such as Cu) by their optical signatures. Finally, it does not require wet chemical methods and precise environmental conditions for sample preparation or analysis, making it well-suited for the constraints of a space environment. For the MHCD-OES analyses of lunar simulants, while a more standard approach would have been to run initial tests on pure compounds, mixtures and doped materials, but then all such tests would only have indirectly pertained to the MHCD analytic capability with real minerals. The analyses of real minerals present

a very different set of challenges because of their complex chemical structure. Described by crystallography the atom-to-atom bonding is quite different than for pure metal oxides. Moreover a given mineral may have different forms (e.g plagioclase v/s pyroxene). Ad-atoms, intrinsic vacancies or many grains comprising a particle all contribute to their distinctiveness and highlight their differences relative to pure materials or even model compounds. Therein the approach taken was to test the MHCD against real minerals first, the rationale being that if analytical merit is not found for the materials of ultimate interest, then all possible preceding tests with simple compounds and doped versions would be needless. Surely it would not be useful to test for elements, concentrations and mixtures that were outside the range of relevance for the targeted minerals. Proceeding on this basis, the simulants do offer a means to test basic analytical figures of merit, which include element detection, concentration measurement, determining linearity and dynamic range, and determining sensitivity to matrix effects.

At the core of each such measure are the two key parameters: precision and accuracy. Analytical precision may be defined as the consistency of measurements whereas optical accuracy refers to closeness to the true value. Both are essential to assessing the nominal analytical figures of merit listed above. Correspondingly specific trials were conducted for these descriptions.

In an attempt to extend the work to other solid samples, MHCD analyses were done on some organic samples in the form of soot as well. The results obtained are included in the Appendix section.

1.2. Thesis Outline:

This thesis summarizes the results obtained while testing MHCD configuration as an analytical device for the analysis of lunar regolith simulants. The next chapter, Chapter 2, reviews the work that has been done in the field of MHCD plasma to provide background information for this research. Chapter 3 describes the experimental set-up used for the analyses while chapter 5 illustrates the MHCD analysis results of the lunar simulants. Some reference analytical techniques were used to confirm the MHCD analyses results, the details of which are discussed in chapter 4. Finally chapter 6, the 'Conclusion Chapter', discusses and summarizes all the findings and future scopes. Some work was also conducted to test the analytical utility of MHCD for the analysis of carbonaceous samples in the form of soot. This work is included in Appendix B of the thesis.

Chapter 2

Literature Review

This chapter aims to provide a brief review of plasmas, their different types and mechanisms of formation. It also briefly summarizes the work that has been done in the field of Micro-Hollow Cathode Discharge (MHCD) plasma so as to provide a background for the analyses in this research project.

Chapter Outline:

2.1 Overview of Plasma

2.2 Classification of Plasmas

2.3 Electrical Breakdown of Gases

2.4 Micro-hollow Cathode Discharge Plasma (MHCD)

2.5 Applications of MHCD plasma

2.6 Summary

2.1 Overview of Plasma:

Plasma is the fourth state of matter following the more familiar states of solid, liquid and gas[14]. It is a quasi-neutral gas with a chemically reactive media that comprises a large number of different species such as electrons, positive and negative ions, metastables, free radicals, gas atoms and molecules in the ground or excited state. The densities and energies of these species depend on factors like the power generator used (applied field, frequency, pulsing properties etc.), type of gas (molecular, atomic, chemical composition, etc.) and on the gas pressures[15] .

2.2 Classification of Plasma:

All varieties of plasma-chemical systems can be divided into two groups – the thermal equilibrium plasma and non-thermal non-equilibrium plasma or cold plasma[15]. The species in thermal plasma are in thermal equilibrium and their temperature ranges from 1000 K to 10000 K. Arc plasma, plasma torches, radio frequency inductively coupled plasma (ICP) are some of the forms of thermal plasmas. Typically thermal plasma is used in areas of material processing and treatment of waste materials[16]. There are some serious drawbacks associated with this form of plasma which include Joule heating, thermal ionization, low excitation selectivity, very high gas temperature, significant energy dissipation and electrode erosion leading to limited energy efficiency [17].

In case of non-thermal plasma, the majority of the electrical energy supplied primarily goes into the production of energetic electrons instead of heating the entire gas stream[16]. Hence the electrons are the main energy carriers while heavier particles like ions, atoms and molecules remain in a lower temperature range of 300 to 1000 K. This form of plasma is generally used for surface treatments such as coating, cleaning or dry etching in the micro-electronics industry, for treatments of Volatile Organic Compounds (VOCs), for generating ozone for water purification, in the field of analytical spectroscopy etc.[17]
Non-thermal plasma has some advantages over the thermal plasma. It represents a more environment-friendly form of plasma. It operates at low temperature which implies that the majority of electrical energy coupled is channeled to the electrons instead of heating the entire gas, which makes it a more energy-efficient technology. The gas temperature being low rules out any special need of quenching. Thus the system does not require a

very high maintenance. Moreover non-thermal plasma offers a very high selectivity to plasma chemical reactions[17]. It is these obvious advantages of non-thermal plasma which led to the rapidly growing interest in the use of this technology from the beginning of this decade. Some of the widely used non-thermal plasma sources are corona discharge, micro-hollow cathode discharge (MHCD), atmospheric pressure plasma jet (APPJ) and dielectric barrier discharge (DBD). The following section briefly discusses the formation of these non-thermal plasma discharges by the phenomena of electrical breakdown of gases.

2.3 Electrical Breakdown of gases:

Electrical breakdown is a complicated process which occurs when an electric field exceeds some critical value[15]. In a plane gap of distance d between two electrodes, connected to a DC power supply, primary electrons are generated near the cathode which produces a very low initial current. The primary electrons, while drifting towards the anode, cause further ionization, generating an avalanche. The avalanche develops both in time and space. The ionization avalanche, i.e electron production per unit length, is described by the Townsend ionization coefficient 'α'. The positive ions thus generated by the ionization process drift towards the cathode and knock out more electrons from the cathode. The probability of the generation of a secondary electron on the cathode by an ion impact is described by the secondary emission coefficient 'γ', also called the third Townsend coefficient. Therefore as soon as the electric field is high enough, resulting in a high Townsend Coefficient 'α', transition to a self-sustained current, i.e breakdown, takes place.

The breakdown condition can be summarized as[16]:

$$\gamma [\exp(\alpha d) - 1] = 1 , \quad \alpha d = \ln(1/\gamma + 1) \qquad (2.3.1)$$

The breakdown voltage can be expressed as:

$$V = Bpd / \{\ln(Apd) - \ln[\ln(1 + 1/\gamma)]\} \qquad (2.3.2)$$

where, V = Breakdown voltage

A, B = parameters which depend on the gas used

p = pressure

d= distance between two electrodes

α = first Townsend Coefficient

γ = third Townsend Coefficient

This relation, which describes the breakdown voltage dependence on the parameter 'pd', is called the Paschen curve. The following figure 2.3.1 represents a Paschen curve which clearly shows that there is a minimum breakdown voltage for a particular value of the product 'pd'. At lower and higher values of 'pd', greater voltage is required for the breakdown phenomena. This is because at a lower value of 'pd', the number of collisions between the electrons and gas molecules will be too few to enable a self-sustaining glow discharge. On the contrary, at higher values of 'pd' the mean free path of the electrons will be sufficiently short such that the electrons cannot reach sufficient energy between two collisions, with the exception being a gap potential so high that streamers might start forming[18]. Therefore it is easiest to operate at the value of 'pd' which gives the minimum voltage.

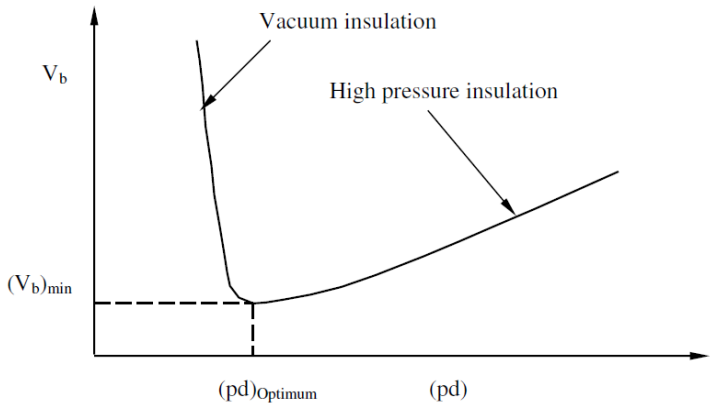

Fig 2.3.1: Paschen Curve [16]

For different gases, the Paschen curve approximately takes the same shape but the minimum positions are shifted.

2.4 Micro-hollow Cathode Discharge plasma (MHCD):

Earlier, low-pressure glow discharge plasmas were of great interest for both fundamental research and in industrial applications, especially in the field of micro-electronics and material processing. But generating these kinds of plasmas involves creating vacuum conditions using expensive vacuum equipment[15]. Therefore significant interests were generated in the development of plasma sources which can operate at atmospheric pressure.

According to Paschen's law, as the gas pressure increases to atmospheric pressure, the characteristic length should be scaled down to 10's to 100's of microns so that the breakdown voltage for plasma formation is minimized[19]. Thus miniaturized discharges in

the form of Micro-hollow cathode discharge (MHCD) can be produced, which have the advantages of low power consumption, high power density, and relatively high electron density while yet operating at atmospheric pressure [20].

In this work, the Micro hollow cathode discharge (MHCD) was considered for the analyses of the solid samples for several reasons. MHCD compared to the corona discharge method produces a more homogenous discharge which results in better uniformity of analysis. In contrast to the geometry of APPJ, which favors the analysis of gas and liquid, MHCD has a geometry which is more suitable for the analysis of solid samples. The MHCD configuration is simpler in construction and is lower in cost by comparison to the DBD configuration. Moreover MHCD uses DC power for its operation which not only ensures an easy control of current and plasma properties but also is much simpler and economical compared to AC and RF power supplies used by the APPJ and DBD configurations respectively[16].

Micro-hollow cathode discharge configuration is a miniaturized version of the classical hollow cathode discharge. The classical geometry has a flat cathode and ring-shaped or a metal pin anode separated from the cathode by a dielectric spacer. Alternatively a thin cathode with a cylindrical opening can also serve as the cathode as shown below[21] in figure 2.5.1 .

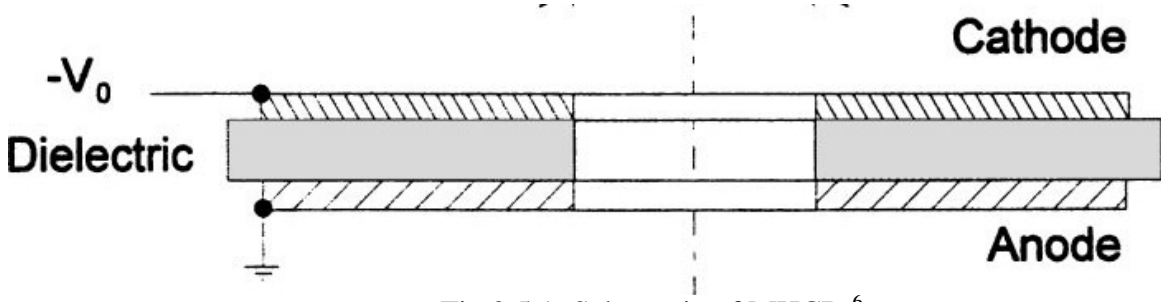

Fig 2.5.1: Schematic of MHCD [6]

The MHCD has been developed by the Schoenbach group for miniaturized structures and integrated assemblies. A relatively low voltage of several hundred volts with current in the range of a few milliamperes is required for the operation of MHCD[22]. The hole diameter ranges from 100 to 200 micrometer for operation in a noble gas environment at atmospheric pressure [16, 21].

The MHCD consists of four discharge modes – the predischarge mode, the hollow cathode discharge mode (voltage decreases with an increase in current i.e. negative differential resistance), the normal glow discharge mode (voltage remains constant with an increase in current) and the abnormal glow discharge mode (to increase current further, an increase in voltage is required, i.e. positive differential resistance)[21]. Generally the MHCD is operated in the negative differential mode. In this mode, the electric field gradient is perpendicular to the hollow axis, accelerates the electrons radially and the electrons perform a pendulum motion between the opposite cathode falls. This results in an increased ionization rate which in turn leads to the decrease in voltage

with increasing current (negative differential resistance). This is called the hollow cathode effect or the Pendel effect[21].

The micro-hollow cathode discharge follows the additional similarity law:

$$V = \mathrm{V}(pD) \qquad 2.5.1$$

where V is the sustaining voltage of the hollow cathode discharge

The lowest value of pD is given by the condition that the mean free path for ionization must not exceed the hole diameter, whereas the condition that the distance between opposite cathodes should not be greater than the length of two fall regions, which determines the upper limit of the pD value[21]. This condition leads to an upper limit of pD slightly greater than 1Torr-cm. This law has been the basis of extending the operating pressure to atmospheric pressure and scaling down the opening in the cathode to the micron range. Normally in an open hollow configuration, electrode cooling and replenishment of the gas already contaminated by sputtered electrode material is ensured.

2.5 Applications of Micro-Hollow Cathode Discharge plasma:

Important applications of the MHCD plasma are as excimer radiation sources, as ionization sources, as charge sources in ion-mobility spectrometry or as excitation and ionization sources in optical emission and mass spectrometry, gas decomposition and gas analysis, surface modification by array micro-structures[23], sterilization in medicine[24] and in electronics[25].

Since this research work aims to use the MHCD as an analytical tool, in this section, applications of MHCD in the field of analytical spectrometry will be highlighted.

As generation of excimer radiation is one of the most important applications of MHCD it will also be discussed briefly.

A) MHCD in excimer radiation:

MHCD consisting of highly stable, high-pressure non-thermal plasma and high-energy electrons are ideal for the formation of excimers[26]. When many such microplasmas are aligned in an array, a large-area excimer radiation source possessing a spectral range from the VUV to near IR can be obtained by selecting the discharge gases. The MHCD can also be used as a photo detector with an extremely high spectral sensitivity[20].

B) MHCD in analytical spectrometry:

The micro hollow cathode plasma has wide applications in analytical spectrometry. With an high electron density in the range of 10^{15}-10^{16} / cm^3 its performance is comparable to that of the classical plasmas used in the field of analytical spectroscopy[23]. A recent surge of interest has been observed in using microplasmas in the field of analytical science. This is mainly due to the 'lab on a chip' concept where these are integrated as spectroscopic detection units. The MHCD plasma easily qualifies for such applications as it requires low input power and operates at high pressure and low gas flow rates. An added advantage is that, being small in size, such a plasma device is portable and can be coupled with any detection instrument[27]. Initially a common drawback of early MHCD designs was the short life span (few hours) due to cathode sputtering. Later, the life span

was extended to a few days by using ceramic insulators and electrodes made of metals with low sputtering rates such as Pt and W.

MHCD coupled with Optical Spectrometry:

The MHCD coupled with optical spectrometry has proved to be an important tool for the analysis of elements and molecular fragments. Miclea *et al.* [27]describes in his publication the use of a MHCD device with an Echelle spectrometer, for the detection of chlorine and fluorine from the decomposition of a chlorofluoro compound (CCl_2F_2, $CHClF_2$). The detection limit was found to be 20 ppb.

MHCD coupled with Gas Chromatography:

Micro-wave induced plasma (MIP) is considered to be the best form of plasma for gas chromatography optical emission spectroscopy (GC-OES). But Braman *et al.* [19]found that direct current discharge has some advantages over the MIP. Direct current discharge uses a more compact power supply than the MIP detector. The microplasma-based detectors have several advantages over typical GC detectors. These can simultaneously detect different elements from a compound, selectively detect every element through its specific emission lines and perform both functions with very low detection limits. In one of his publications Miclea *et al.* [28]describes using a MHCD, operated at atmospheric pressure, with a gas chromatograph to analyze halogenated hydrocarbons. Halogens and sulfur could be detected as the halocarbons eluted from the GC. The reported detection limits were 35 pg, 100 pg, 155 pg, and 295 pg for F, Cl, Br and S, respectively[28].

MHCD coupled with Mass Spectrometry:

A MHCD unit was also coupled with a quadrupole mass spectrometer to serve as a dissociation and ionization source for the analysis of halogenated hydrocarbons. The measured element ion signal ratios are equivalent to the element ratios in the molecules and the concentration ratios of the species which forms the basis of its calibration by an internal standard. The detection limit in this case was 40 pg/s for Cl^+ which demonstrates the device to be very effective for gas analysis[29].

Thus it can be seen that the increasing demand for miniaturized instruments has led to a significant development of coupling MHCD plasmas with other analytical equipment to form a total-analysis-system. The greatest advances are with GC because small gas chromatographs are already produced by different companies. Further system expansion awaits the development of miniaturized Echelle spectrometers and mass spectrometers.

2.6 Summary:

This chapter gives a brief overview of the work that has been done in the field of plasma. It discusses the different plasma types and configurations that have widely different properties and are used in diverse fields. The micro-hollow cathode discharge plasma (MHCD) is one such type which has characteristics that suit the nature of this work, specifically the analysis of solid samples.

From the literature, it is evident that MHCD plasma has varied applications in the field of analytical spectroscopy. Todate it has been coupled with some other detection

instruments and used mainly for gaseous analytes. This research work explores the use of a MHCD plasma source as an independent analytical device, for the analysis of inorganic solid samples in the form of lunar regolith simulants.

Chapter 3

Experimental Set-up

This chapter discusses the experimental work that was involved in this research. It provides a detailed description of the hardware set-up and the spectrometer used.

Chapter Outline:

3.1 Sample Preparation

3.2 Hardware set-up

3.3 Spectrometer

3.4 Summary

3.1 Sample Preparation

The seven lunar regolith simulant samples Synthetic Anorthite, CL2 Concentrate. (Plagioclase Concentrate), Chenobi, JSC-1, JSC-1A, NU-LHT-2M and Ro-Tails were directly obtained from NASA and did not require any special sample preparation. All the simulant samples were ground by a mortar and pestle to bring them to a size convenient for the MHCD-OES analysis

3.2 Hardware Setup:

3.2.1 Overall set-up

The experimental apparatus consists of a chamber with the MHCD unit, a DC power supply and spectrometer for capturing atomic/molecular optical emission. High-purity (99.95%) Argon is used as the carrier gas with flow rates of 2–3 liter per min (LPM) at

standard conditions (293 K, 0.1 MPa). The flow of the gas is governed by a multigas-programmer MKS model 647B. Micro-plasma analysis generated an associated optical emission spectrum from each sample under an argon gas background with an applied DC voltage ranging between 1100 and 1500 V. A 'Stellar Net Black Comet Concave Grating spectrometer' was used to record the optical emission spectra of the lunar simulant samples. Figure 3.2.1 shows the experimental schematic that comprises the optical collecting system (spectrometer, fiber optic cable and lens) and the MHCD element.

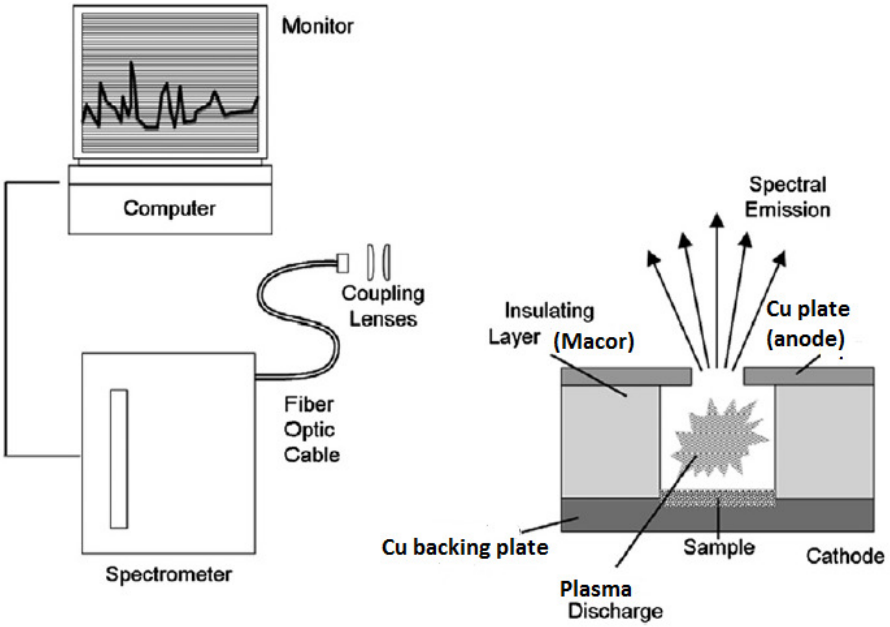

Fig 3.2.1: Experimental schematic of the optical set-up and the micro-hollow cathode discharge element

3.2.2. MHCD element

As shown in figure 3.2.2.2 (a), a set of two copper discs (the two electrodes) and a Macor disc (the dielectric) were used. The anode Cu disc and the Macor dielectric spacer had equal hole diameters (of 279.4μm). The other copper disc or the backing plate (anode) was of a smaller diameter compared to the other two and had a small depression of diameter 279.4μm (instead of the hole) punched at its center to hold the sample charge. The three discs were assembled in a sandwich style, with the macor disc at the centre, such that the hole, annulus (i.e macor disc) and depression were aligned. The micro-plasma generated in the annulus eroded the solid simulant held in the depression and electronically excited the elements in the resulting plasma, thus generating a signal for compositional analysis of the simulant.

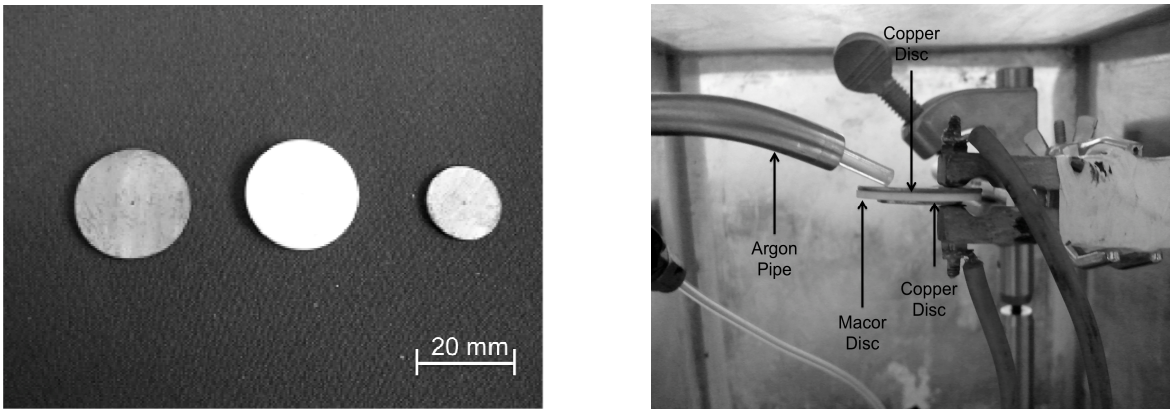

(a) (b)

Fig: 3.2.2.: (a) the two Cu discs and the macor disc (b) Cudisc/macor disc assembly for experimentation

3.2.3. Analysis Mechanism:

For the micro-hollow cathode discharge analysis of solid samples, an initial plasma is generated (in the micro-hollow) by ionizing the Argon gas (the ambient gas in this case) and the resulting Ar ions, bombard the solid material deposited on the backing plate, "knocking off" atoms from the sample surfaces. These atoms become electronically excited in the plasma and emit emission wavelengths characteristic of the particular element. This UV-Visible emission is collected by the spectrometer as the MHCD-OES spectrum. Argon is the preferred gas for the sputtering action due to its mass.

For all the experiments performed with the lunar regolith simulants a mass of 1mg of sample was placed at the center of the backing plate, to be used for MHCD-OES analysis. This is not however the material mass analyzed. The mass of soot analyzed is that deposited within the area equal to that projected by the hollow annulus, as only this surface is accessible to the sputtering action of the plasma. This projected area yields an analyzed mass of order 1μg with an associated count rate yielding a S/N ratio of greater than 100 for tens of spectra (generally greater than 30) for a single sample charge.

3.3 Spectrometers:

The MHCD plasma analysis technique, based on the principles of atomic emission spectroscopy, requires the use of a spectrometer for collecting the atomic emission signals and generating atomic emission spectra which forms the very basis of the analysis. The fiber optic cable relaying the signal to the spectrometer is positioned in

such a way so as to be able to collect the emission wavelengths, and the spectrometer is coupled to a computer which processes the collected signals.

Out of the many different models of spectrometers manufactured by Stellar Net, this work involved the use of 'Black-Comet Concave Grating Spectrometer' which is a f/2 flat-field spectrograph[30]. This model uses an aberration-corrected 40mm diameter concave grating which helps to improve spectral shapes by reducing comma and astigmatism found in plane spectrograph designs. As the spectrograph architecture does not involve use of a mirror and uses a holographic grating instead of a rough-surfaced normal-ruled grating, there is an enormous reduction in the stray light effects.

The spectrograph uses a 2048-pixel CCD detector with a wavelength range of 190-850nm. It has a very low power consumption of 100mA at 5VDC. Its uses selectable integration time, ranging from 1ms to 65s. It has a very high signal to noise ratio of 1000:1. In order to precisely control optical resolution, a slit is permanently installed in the spectrometer entrance. This allows the instrument to maintain resolution when a different fiber size is connected. Optical resolution determines the instrument's ability to resolve adjacent spectral peaks which (for example) relates to identifying elemental composition via optical emission. The instrument has an optical resolution of 0.45nm.These instruments are exceptionally robust with no moving parts and are packaged in a small rugged metal enclosure of size 2.75 X 4X 6 inch, which makes the system very portable.

For the experiments that were performed with the lunar regolith simulants, a suite of 40 spectra were acquired per test and 10 tests were conducted per sample to confirm the results. An integration time of 200ms was used. Most of the spectra collected would show similar relative peak intensities, highlighting reproducibility of the MHCD technique. But sometimes due to the arc formation or due to sample getting exhausted, false spectra might get generated which would have widely different relative peak intensities than the other spectra. Such spectra were discarded and an average of the rest of the spectra was calculated to represent the composition of the sample as determined by MHCD-OES.

3.4. Summary:

This chapter provides all the experimental details of this research. It provides the description of the hardware set-up and the MHCD element that were used for the lunar regolith simulants. It also includes the detailed specifications of the spectrometer used.

Chapter 4

Reference Techniques Used

This chapter discusses the other analytical techniques (other than MHCD-OES), which provided the reference compositional analyses data of the lunar regolith simulants for comparison with MHCD-OES analyses, and therefore helped in gauging MHCD-OES as an analytical technique.

The following reference techniques have been used in this research:

- Scanning electron microscopy (SEM) along with Energy Dispersive X-ray Spectroscopy (EDS)
- Inductively Coupled Plasma Optical Emission Spectroscopy (ICP-OES)

Chapter Outline:

4.1. Scanning Electron Microscopy (SEM)

SEM was applied to gain a better understanding of the surface morphologies and surface characteristics of the different simulants and to observe the degree of heterogeneity in each. Most importantly SEM was used to generate characteristic X-rays from the samples which were analyzed by the EDS detector to determine the composition of the sample.

4.1.1. Overview of the Technique

SEM uses a focused, high-energy electron beam to scan small areas of solid samples. Signals produced are in the form of secondary electrons, back-scattered Auger electrons and characteristic X-rays. Both secondary electron and backscattered electron signals are used for imaging of the sample. Secondary electrons can produce a high-resolution topographical image of the sample surface with spatial resolution as high as 1 nanometer for some instruments, but 4 nm is typical for most. Backscattered electrons (BSE) can also provide qualitative information about the near-surface distribution of different elements in the sample, whereas characteristic X-rays are used for accurate compositional sample analysis.

4.1.2. Equipment Specifications:

The SEM instrument used for this research was a Hitachi S-3500N. It has the most common electron gun which employs a tungsten filament that is resistively heated to nearly 3000K until electrons have sufficient energy to overcome the work-function energy barrier (thermionic emission).

The S-3500N has options of working with both the conventional high-vacuum mode and variable-pressure mode. The variable-pressure mode allows the microscopy of wet, oily and nonconductive samples in their natural state without the need for conventional sample preparation and coating. Energy dispersive X-ray microanalysis can be carried out on a sample in both high-vacuum and variable-pressure modes. Since the lunar simulant samples were partially non-conductive, the variable-pressure mode was used for their analyses.

Instrument Conditions used for sample characterization and analysis:

- Secondary Electron resolution: 3.0 nm (High-Vacuum mode)
- Accelerating Voltage : 20keV
- Magnifications:

  Readings were taken for 2 sets of magnification,

  i) in a range of 350X - 500X

  ii) in a range of 1.2kX –1.8kX

  For the Ro-Tails sample it was difficult to make observation in the magnification range of 350 X – 500X , due to its slightly different morphology. Therefore Ro-Tails readings were recorded at magnifications 1.8kX and 5kX.
- Specimen size: 20mm diameter
- Specimen stage : 100mm by 50mm (5-axis motorised)
- Peltier stage: minimum temperature - 20 degrees centigrade.

4.1.3. SEM Images: The following SEM images represent the surface of the seven lunar regolith simulants at low and high magnification.

Synthetic Anorthite

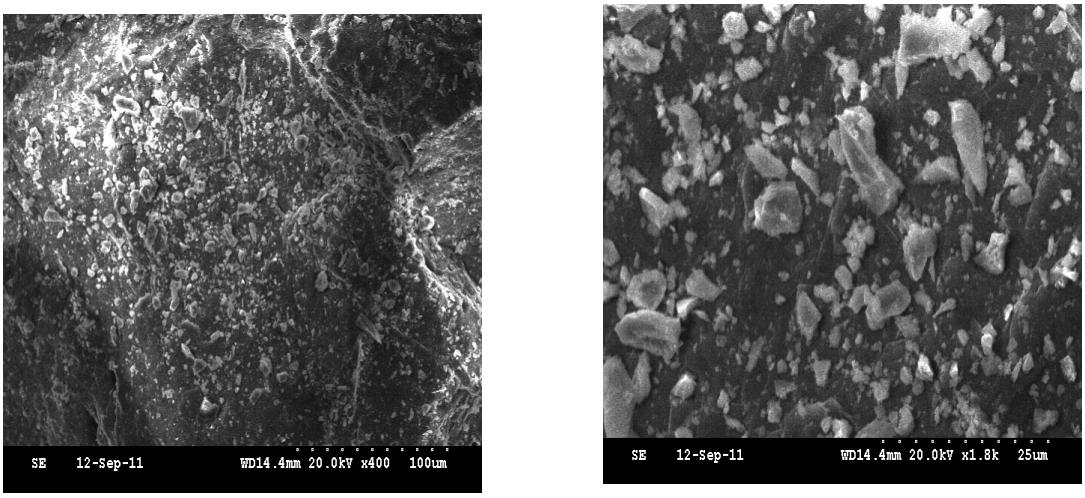

(a) (b)

Fig.4.1.1: SEM images of Synthetic Anorthite at a) 400X and b) 1.8kX magnification

CL2CON. (Plagioclase Concentrate)

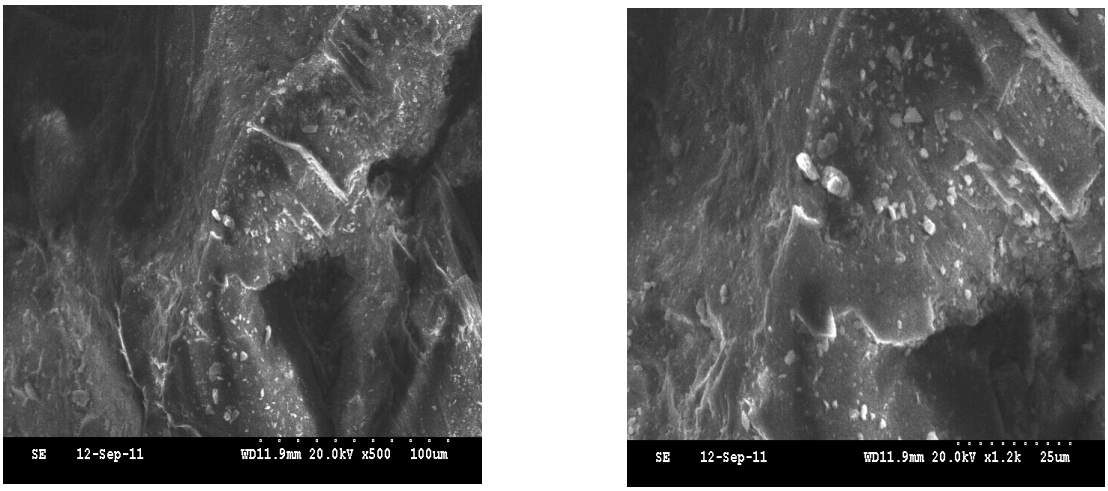

(a) (b)

Fig.4.1.2: SEM images of CL2CON. (Plagioclase concentrate) at a) 500X and b) 1.2kX magnification

Chenobi:

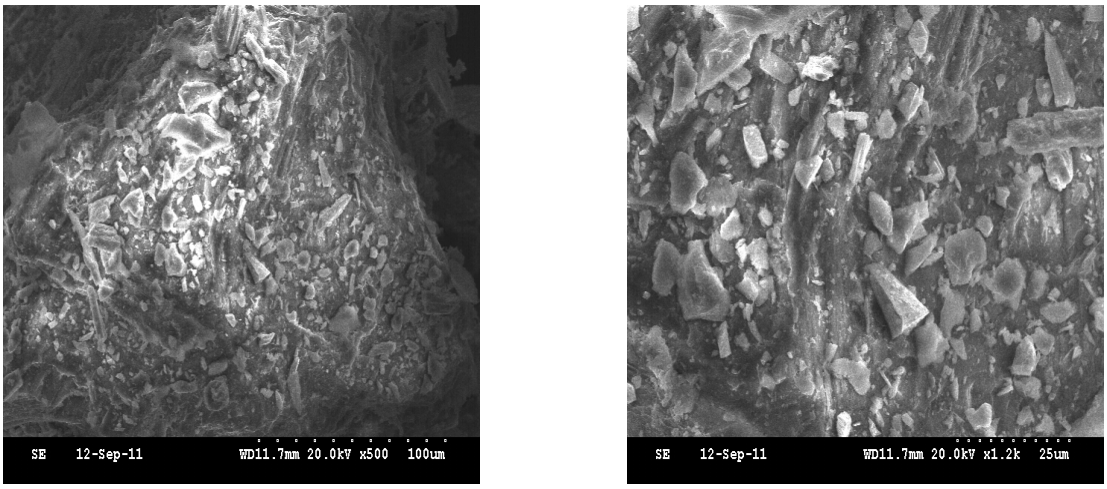

(a) (b)

Fig.4.1.3: SEM images of Chenobi at a) 500X and b) 1.2kX magnification

JSC-1:

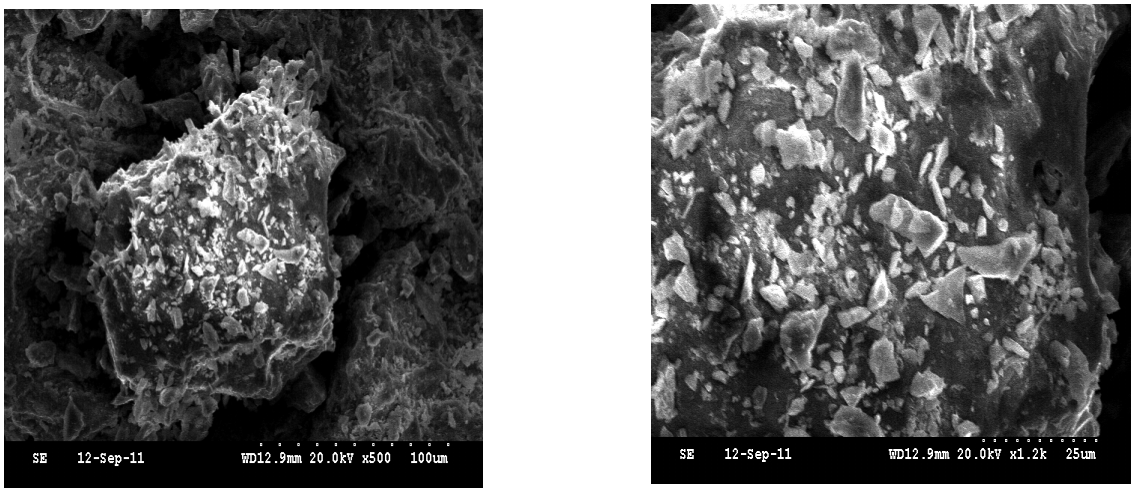

(a) (b)

Fig.4.1.4: SEM images of JSC-1 at a) 500X and b) 1.2kX magnification

JSC-1A:

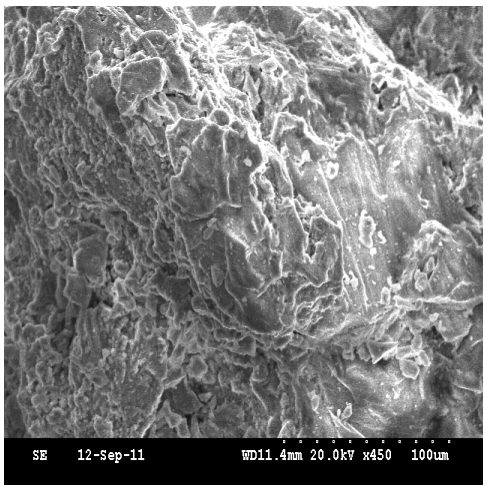

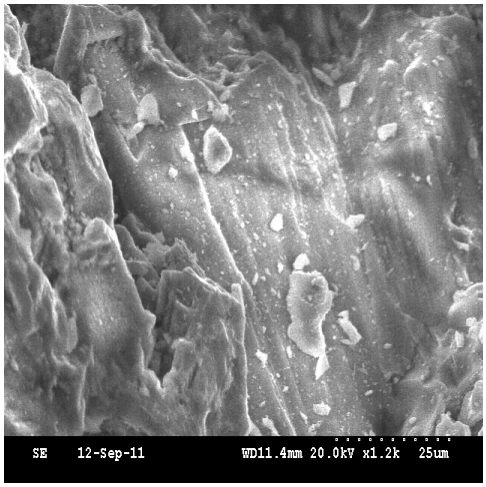

(a) (b)

Fig.4.1.5: SEM images of JSC-1A at a) 450X and b) 1.2kX magnification

NU-LHT-2M:

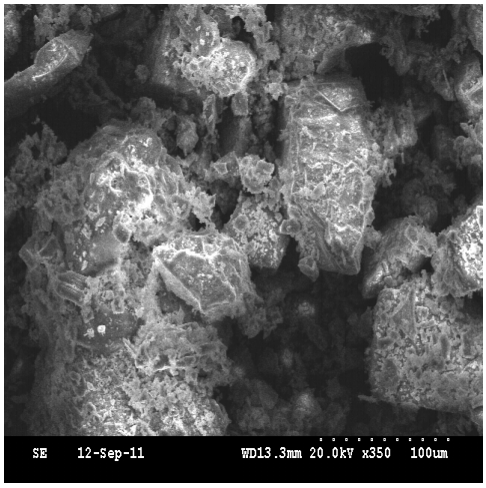

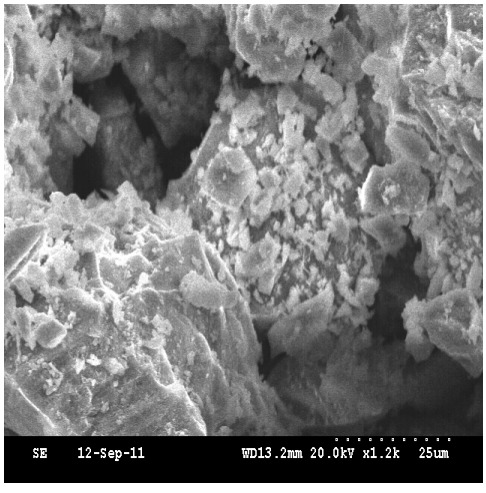

(a) (b)

Fig4.1.6: SEM images of NU-LHT-2M at a) 350X and b) 1.2kX magnification

RO-Tails (Pyroxene Concentrate):

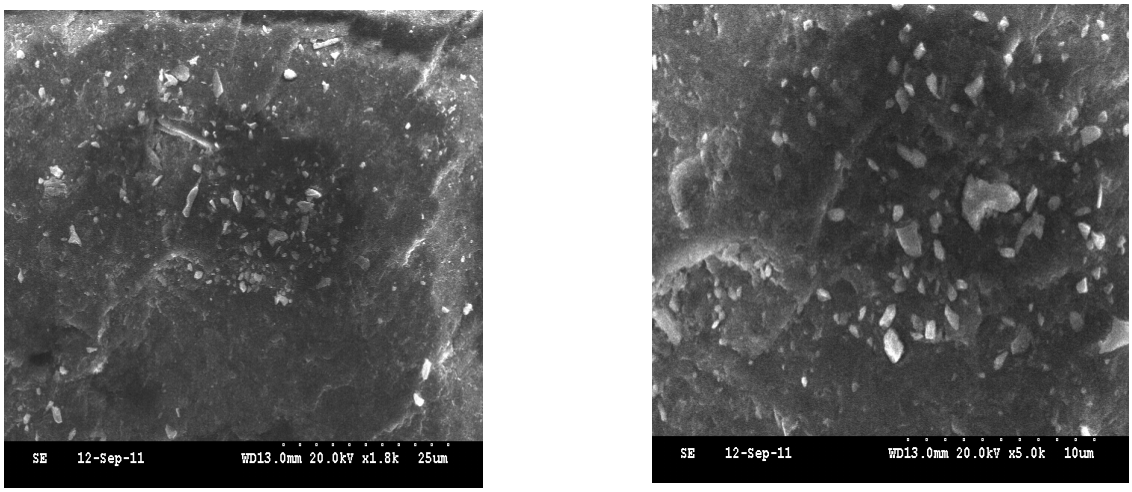

(a) (b)

Fig.4.1. 7: SEM images of RO-Tails at a) 1.8kX and b) 5.0kX magnification

4.2. Energy Dispersive X-Ray Spectroscopy (EDS/EDX):

4.2.1 Overview of the technique:

Energy Dispersive Spectroscopy (EDS) is a standard procedure for the identification and quantification of the elemental composition of sample areas as small as a few cubic micrometers based on the detection of the characteristic X-rays emitted by the elements present within the sample (when subjected to the electron beam within the SEM).

This technique was used to find the elemental composition of the seven lunar regolith simulants to serve as a reference for the data obtained by the micro-hollow discharge plasma analysis. Thus it would serve to validate the applicability of micro-hollow discharge plasma as an analytical technique for solid samples.

4.2.2. Equipment Specifications:

For the EDS analysis a Princeton Gamma Tech Prism Digital Spectrometer was used. The conditions used are the same as that of the SEM conditions.

4.2.3. Analysis Results:

Analysis results are reported as oxides by general convention (e.g., Si as SiO_2). It is common to report rock compositions in this manner since most elements in such materials exist in the oxide form. This method also makes it easier to compare with other analysis results in the literature. A summary of the analysis data for the lunar simulants thus obtained is given below:

Elemental Oxide Weight Percentages (EDS data)

	Synthetic Anorthite	Cl2.CON (Plagioclase Concentrate)	Chenobi	JSC-1	JSC-1A	NU-LHT-2M	Ro-Tails
SiO_2	48.81	49.58	48.42	60.96	53.39	44.49	38.45
TiO_2	-	-	-	-	-	2.07	-
Al_2O_3	27.41	29.94	29.64	4.18	20.81	14.34	6.05
Fe_2O_3	-	-	-	-	-	-	-
FeO	1.46	2.26	1.79	11.20	-	19.00	23.74
MgO	-	1.63	.34	21.57	-	4.25	29.01
CaO	20.80	15.72	18.70	2.09	25.80	11.56	.91
Na_2O	1.52	.87	1.11	-		3.10	-

Table 4.2.1: Composition of the lunar regolith simulant samples- as determined by EDS

4.2.4. Drawbacks of the Technique

Using EDS, rapid elemental analyses of small features and two-dimensional spatial mappings for elements can be done. But this technique was not fully suitable for the analyses involved in this research due to the following reasons:

Semi-quantitative technique:

- As mentioned previously, the main objective of using EDS technique was to generate reference data for the MHCD-OES analyses. But since it is a semi-quantitative technique, EDS itself requires a set of standard data to generate accurate results. Therefore it was not fully capable of serving as a reference technique for the MHCD-OES analysis.

Simulant Heterogeneity:

- Most of the simulants are heterogeneous in nature and their composition varies throughout the sample. Analysis of a small portion in a near-surface region will not be representative of the average 'bulk' composition.

Varied Sample Particle Morphology:

- A flat-surfaced sample is preferred for EDS such that the working distance is the same throughout and the signal emitted by the sample surface reaches the detector without being blocked by any other particle. The detector counts the signal and on that basis predicts the composition. As can be seen from the SEM images the

lunar regolith simulant samples do not have a flat surface and therefore cannot be analyzed by EDS.

The EDS results were checked against the data later sent by NASA. These did not match very well, proving that the results obtained by EDS analyses were inadequate. Thus finally the data sent by NASA (sent during later months of the project) served as the reference for the results generated using MHCD-OES. As the analyses data sent by NASA did not include the analysis result of one of the simulants, Chenobi, ICP-AES analysis was done on it to determine its composition; the ICP-AES determined data can serve as the reference data for Chenobi. ICP analysis was also done on another sample, Synthetic Anorthite, and the results compared with its data from NASA to confirm the applicability of ICP analysis as a reference analytical technique for the lunar regolith simulants. The analyses results matched very well for the sample Synthetic Anorthite thus validating the applicability of ICP-AES as an analytical technique for the analysis of lunar simulant samples.

4.3. Inductively Coupled Plasma Atomic Emission Spectroscopy (ICP-AES):

4.3.1. Overview of the Technique:

Inductively coupled plasma atomic emission spectroscopy (ICP-AES) also known as inductively coupled plasma optical emission spectroscopy (ICP-OES) is an analytical technique based on emission spectroscopy. It uses inductively coupled plasma to electronically excite atoms and ions from the sample, which emits electromagnetic radiation of wavelengths characteristic to the particular element.

4.3.2. Equipment Specifications:

For ICP analysis a Perkin-Elmer Optima 5300DV ICP-AES was used. About 100mg of each simulant was analyzed in each case. Since the sample was solid, it was ground to powdery form and dissolved by lithium metaborate fusion. In the Perkin-Elmer Optima 5300DV ICP-AES, the solution to be characterized is nebulized into a fine aerosol and introduced into argon plasma with a temperature ranging from 7000-10,000 degrees Kelvin, (a true thermal plasma).

4.3.3. Analyses Results:

The ICP-AES analysis results were used as the reference values for Chenobi and Synthetic Anorthite. The ICP-AES results are tabulated as follows:

Elemental Oxide Weight Percentages (ICP-AES data)

	Chenobi	Synthetic Anorthite
SiO_2	48.2	45.5
Al_2O_3	29.34	39.10
Fe_2O_3	1.76	.08
MgO	.47	.18
CaO	16	14.34
Na_2O	4.23	1.07

Table 4.3.3.1.Compositional analysis of Chenobi & Synthetic Anorthite using ICP-AES

4.4. Summary:

This chapter illustrates the different analytical techniques that have been used as reference techniques for the MHCD-OES analyses of the lunar regolith simulants. The MHCD-OES analyses data were matched against these reference data to validate MHCD-OES analysis as an appropriate analytical tool to analyze lunar regolith samples.

SEM was used to study the surface morphologies and the heterogeneity of the different simulants in order to understand the varied nature of the seven samples. EDS was conducted to find the chemical composition of the samples. But it was observed that EDS, being a semi-quantitative technique was inappropriate for the analyses of the lunar simulants. Moreover the simulants as predicted by the SEM analysis were heterogenous in particle mineral content and so the results obtained by EDS were not representative of the entire sample. Ultimately compositional analysis data sent by NASA for the six out of seven simulants served as the reference for the data generated by micro-hollow plasma.
ICP-OES was also conducted for the composition analysis of two of the simulants so as to validate the data sent by NASA and also to obtain the analysis data for the seventh simulant for which no compositional data was available.

Chapter 5

Results and Discussions

Micro-Hollow Cathode Discharge (MHCD) plasma was used for the analysis of seven lunar regolith simulants. The spectral signatures obtained for each of the simulant formed the basis of the compositional analysis of the simulants. MHCD-OES was also tested for the two key parameters-analytical precision and accuracy. Analytical Precision is the consistency of measurements whereas Optical Accuracy refers to the closeness to the true value. Both of these parameters are important for assessing the nominal analytical figures of merit such as element detection and concentration, linearity and dynamic range and the sensitivity to matrix effect.

The MHCD-OES analysis data has been illustrated in two formats. The first is in the form of scaling factors. The scaling factors encompass both instrumental response and proportionality of signal to element concentration within a particular mineral, and therefore can directly test the matrix effect which arises due to the different crystallography or different bonding of the element of interest in different minerals. The second approach for illustrating the MHCD response directly evaluates the OES signal as a function of specific element concentrations across the range of minerals (simulants) tested. Such signal versus concentration analysis constitutes the normal analytical curves for illustrating technique/instrument linearity and dynamic range

For all the experiments performed with the lunar simulants, one common procedure was followed. The samples were loaded in the depression of the backing plate (here one loading is referred to as a 'sample charge') and analyzed using microplasma. A set of forty spectra is collected with an interval of 10ms between any two spectra. This set of forty spectra constitutes a single 'series' of spectra. For a particular simulant such tests were repeated ten times, and ten series of spectra with four hundred total spectra were collected. An average of all the four hundred spectra was taken for performing all the analyses.

Chapter Outline:

5.1. MHCD-OES analyses results

5.2. Analytical Precision

5.3. Analytical Accuracy

5.4. Matrix Effect

5.5. Dynamic Range and Linearity

5.6 Summary

5.1. MHCD-OES Analyses Results:

A summary of all observed atomic and diatomic species produced by micro-plasma analysis of the seven samples, their excited state emission wavelengths and designated spectral transitions are tabulated in table 5.1. 1. This information was used in the analysis and interpretation of the emission spectra graphs.

Elemental species	Wavelength (nm)	Spectral Transitions
SiO^{31}	221	$A^1\Pi$-$X^1\Sigma$
Si^{32}	213	$^1F^0$-^1D
Si^{31}	252	$^3P^0$-^3P
Si^{31}	288	$^1P^0$-^1D
Mg^{33}	280	$^2P^0$-^2S
Mg^{33}	285	$^1P^0$-^1S
Mg^{34}	518	$^3P^0$-^3S
Fe^{32}	239	$^5P^0$-^5D
Fe^{35}	260	$^5G^0$-^5F
Fe^{33}	375	$^5F^0$-^5D
Ca^{33}	393	$^2P^0$-^2S
Ca^{33}	559	$^3D^0$-^3D
Na^{33}	589	$^2P^0$-^2S

Table 5.1.1: List of atomic and diatomic species, their corresponding wavelengths and spectral transitions

The spectra of the seven lunar regolith simulant samples are reported and discussed in this section. Apart from these sample-dependent transitions, the presence of a copper

(Cu) peak at 324nm was observed in all the seven spectra. As all the samples are known to be devoid of Cu, the occurrence of this atomic line is indicative of the existence of Cu produced by minor sputtering of the Cu electrodes. Also it should be mentioned that in case of the spectra of all the simulants (all of which have both Al and Ca) the very low intensity spectral line of Aluminum (Al) at 394nm is superimposed on the much stronger spectral line of Calcium at 393nm given the instrumental resolution of ~1nm. Thus the Al peak could not be observed for any of the simulants.

It should be noted that the majority of the information about the description of the simulants have been provided by NASA.

I) Synthetic Anorthite:

These are crystals formed by annealing glass having composition $CaAl_2Si_2O_8$ [36]. Typically this produces a pure plagioclase feldspar mineral mainly consisting of anorthite (a type of plagioclase feldspar), though some albite mineral ($NaAlSi_3O_8$) might also form. The ratio of anorthite to albite (Ca/Na) is greater than 90%. Its nominal composition as provided by NASA is shown in table 5.1.2:

Oxides	Wt%
SiO_2	45.50
Al_2O_3	39.10
CaO	14.34
Na_2O	1.07

Table 5.1.2: Synthetic Anorthite Composition

The spectra of Synthetic Anorthite, (as can be seen from figure 5.1.1) as obtained using the atmospheric pressure micro-plasma configuration, show prominent Si and Ca peaks due to the high concentration of Si and Ca present. Mg and Fe do not form an intrinsic part of the molecular structure of the mineral present, as can be observed from its chemical composition in table 4.4. But these being present as impurities in the sample give rise to the low-intensity Mg and Fe peaks in the spectra.

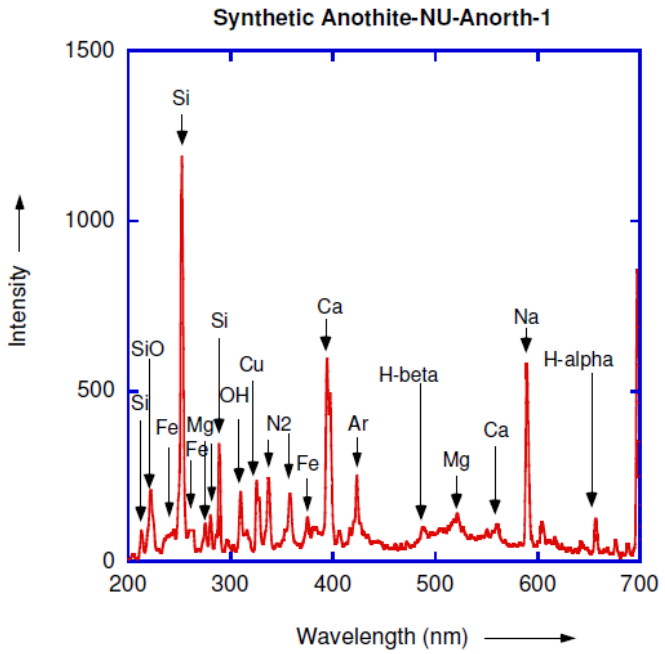

Fig 5.1.1: MHCD-OES spectrum of Synthetic Anorthite

II) **Cl2CON. (Plagioclase concentrated):**

This simulant consists of about 95%-98% of plagioclase feldspar. It consists of both the forms of plagioclase mineral-Anorthite ($CaAl_2Si_2O_8$) and Albite ($NaAlSi_3O_8$), in the ratio of 82%. Hence the Na content is more in this sample compared to the previous one.

Its composition is as listed in table 5.1.3:

Oxides	Wt%
SiO_2	50.67
Al_2O_3	31.61
CaO	14.26
Na_2O	3.46

Table 5.1.3: CL2CON.(Plagioclase Concentrate) composition

Since the main constituent of CL2-CON is Plagioclase ($NaAlSi_3O_8$ – $CaAl_2Si_2O_8$), the spectra reports high intensity emission peaks of Si and Ca, similar to the case of Synthetic Anorthite (as can be seen from figure 5.1.2). But contrary to the previous spectrum, this spectrum reports a Na peak of higher intensity. This is indicative of the analytical range of the MHCD-OES device which can detect the difference in the Anorthite to Albite (Ca/Na) ratios in the two cases.

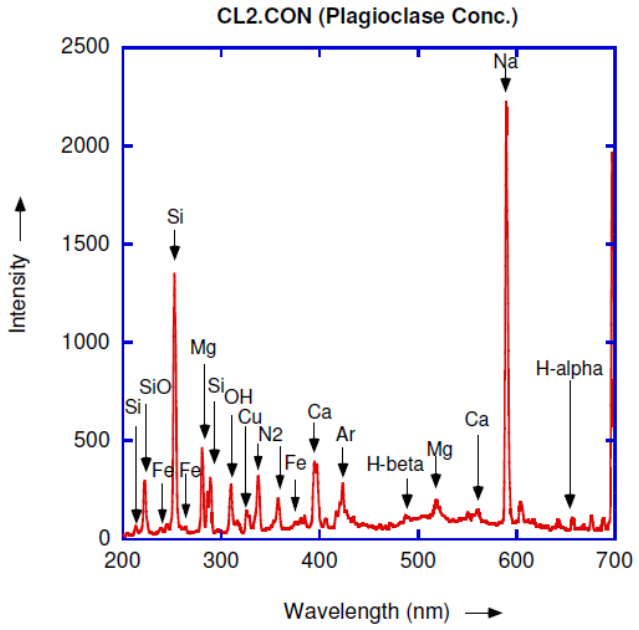

Fig 5.1.2: MHCD-OES spectrum of CL2CON. (Plagioclase Concentrate)

III) Chenobi

Chenobi is a lunar highland, anorthosite-based simulant[37]. Anorthosite is an intrusive igneous rock characterized by predominance of plagioclase feldspar ($NaAlSi_3O_8$ – $CaAl_2Si_2O_8$). The anorthosites are ground, melted and mixed to form Chenobi. Thus Chenobi is 95% pure plagioclase. The ratio of Anorthite to Albite (Ca/Na) is 78% in this case. A small percentage of pyroxene (Ca, Mg, Fe Silicate) is also present. Its chemical composition as found by ICP-AES is tabulated as shown in table 5.1.4:

Oxides	Wt%
SiO_2	48.2
Al_2O_3	29.34
CaO	16
MgO	.47
Fe_2O_3	1.76
Na_2O	4.23

Table 5.1.4: Chenobi composition

As Chenobi mainly consists of plagioclase, its MHCD-OES spectrum has high-intensity peaks from Si and Ca. Mg and Fe present in the form of pyroxene mineral, in the sample, results in low-intensity spectral lines. In this case, the Anorthite to Albite ratio (Ca/Na) value is lower than the other plagioclase-based simulants described above. This fact is confirmed by the Chenobi spectrum obtained by the MHCD-OES analysis as shown in figure 5.1.3.

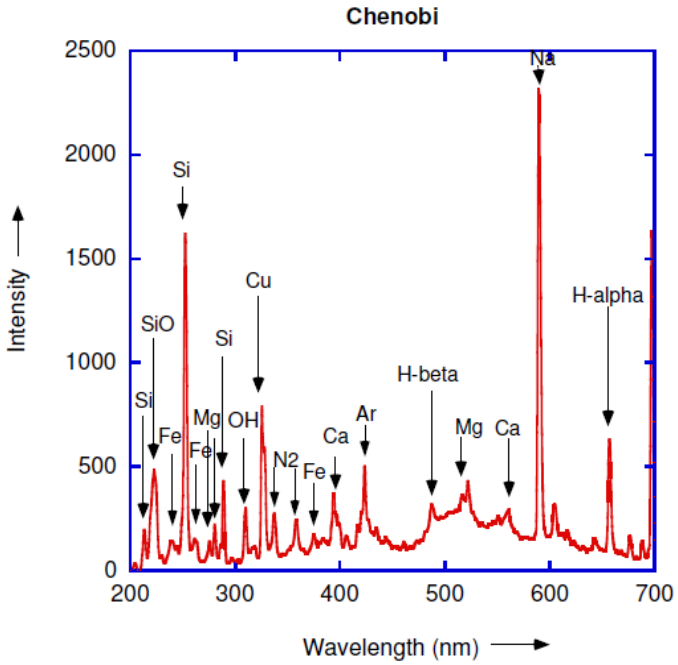

Fig 5.1.3: MHCD-OES spectrum of Chenobi.

IV) JSC-1:

JSC-1 is a lunar simulant derived from volcanic ash of basaltic composition. The composition of the JSC-1 sample corresponds to the composition of the lunar mare soil which is rich in iron[38]. It consists mainly of three minerals–plagioclase ($NaAlSi_3O_8$ – $CaAl_2Si_2O_8$), pyroxene (Ca, Mg, Fe Silicate) and olivine ($[Mg, Fe]_2SiO_4$) and other minerals such as ilmenite, chromite , and traces of clay in minor quantities. The simulant contains a high percentage of glass similar to the lunar mare soil which has considerable glass content owing to micro-meteoritic impact taking place. The major element composition of JSC-1 is summarized table 5.1.5:

Oxides	Wt%
SiO_2	47.71
Al_2O_3	15.02
Fe_2O_3	3.44
FeO	7.35
MgO	9.01
CaO	10.42
Na_2O	2.70

Table 5.1.5: JSC-1 Composition

.

Since plagioclase, pyroxene and olivine – all the three minerals are present in this simulant, the concentrations of Fe and Mg are also much higher in this case compared to the previous simulants. Correspondingly it is observed from the spectrum (as shown in figure 5.1.4) that the Fe and Mg emission peaks are of much higher intensity in this case compared to the previous cases, especially the Fe peak at 239nm and the Mg peak at 280 nm. These high-intensity spectral lines represent the higher concentrations of Fe and Mg in JSC-1. The fact that the MHCD-OES detector could detect this increase in concentration, once again, highlights the analytical trueness of the technique.

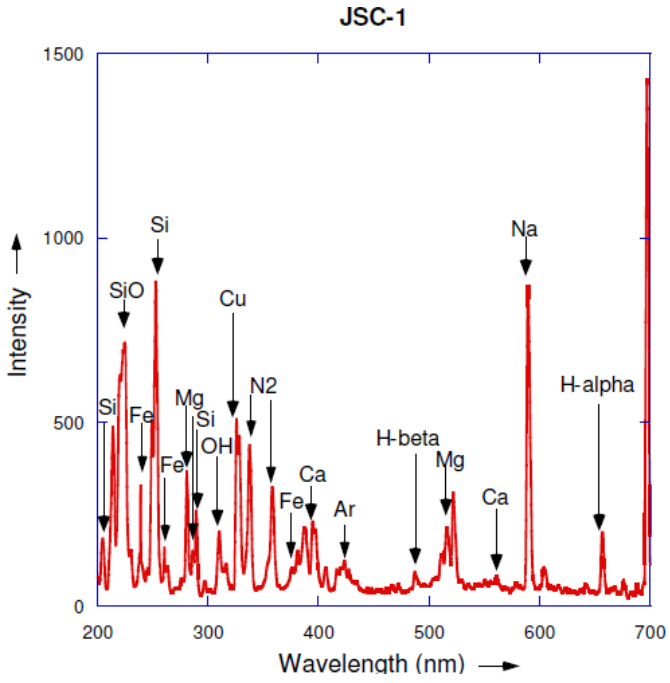

5.1.4: MHCD-OES spectrum of JSC-1

V) JSC-1A

JSC-1A is a part of the suite of three simulant materials JSC-1AF, JSC-1A, JSC-1AC[39]. It is very close in composition and grain size to JSC-1 simulant and is mined from the cinder quarry of the Merriam crater located in San Francisco. This simulant also resembles the regolith in lunar mares. Plagioclase feldspar ($NaAlSi_3O_8$ – $CaAl_2Si_2O_8$) is the major mineral present along with basaltic glass. Olivine and calcium pyroxene are present in minor quantities, whereas titano-magnetite and chromite are present in minor to trace amounts. Around 40% of glass is also present. It is a fairly heterogeneous sample and can be categorized as the second most complex sample (among the seven lunar simulants), after NU-LHT-2M. Composition variation can be observed with differing particle sizes. Its chemical composition is summarized in the following table 5.1.6:

Oxides	Wt%
SiO_2	46.67
Al_2O_3	15.79
Fe_2O_3	12.5
FeO	8.17
MgO	9.39
CaO	9.90
Na_2O	2.83

Table 5.1.6: JSC-1A Composition

JSC-1A has a composition very similar to that of JSC-1. This fact is supported by the spectra obtained (as shown in figure 5.1.5), which shows the similarities of this spectrum to the JSC-1 spectrum in terms of the relative intensities of the peaks.

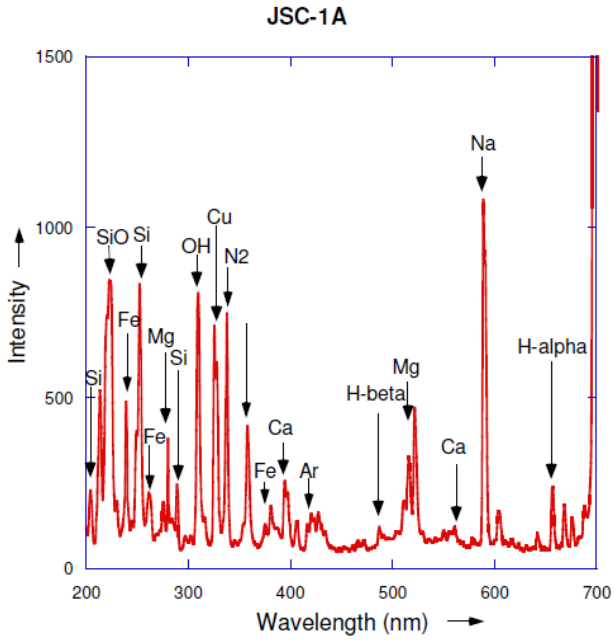

5.1.5: MHCD-OES spectrum of JSC-1A

VI) NU-LHT-2M:

NU-LHT-2M is a highland regolith simulant. It is powdery in nature and comprises grounded rocks such as anorthosite and norite[40]. The anorthosite and norite are obtained from a Stillwater-layered intrusion and the glass material is prepared synthetically using a plasma melter facility.

It consists of aluminosilicates such as calcium-plagioclase ($CaAl_2Si_2O_8$), orthopyroxene (Fe, Mg silicate), and clinopyroxene (Ca, Mg, Fe Silicate). It also has a considerable amount of glass material. Minor or trace amounts of minerals such as ilmenite, β-tricalcium phosphate (whitlockite), pyrite and fluor apatite are also present. No asbestos is present and quartz content is less than 2%. The presence of so many minerals makes it a highly heterogeneous simulant. Its composition varies with particle size fraction.

The composition of the simulant is given in table 5.1.7:

Oxides	Wt%
SiO_2	46.7
Al_2O_3	24.4
CaO	13.6
MgO	7.90
Fe_2O_3	4.16
Na_2O	1.26

Table: 5.1.7: NU-LHT-2M composition

NU-LHT-2M consists of both plagioclase and pyroxenes. Thus Mg and Fe peaks should be more prominent in this case compared to the first three cases which were plagioclase dominated. This is illustrated by the NU-LHT2M spectra as shown in figure 5.1.6.

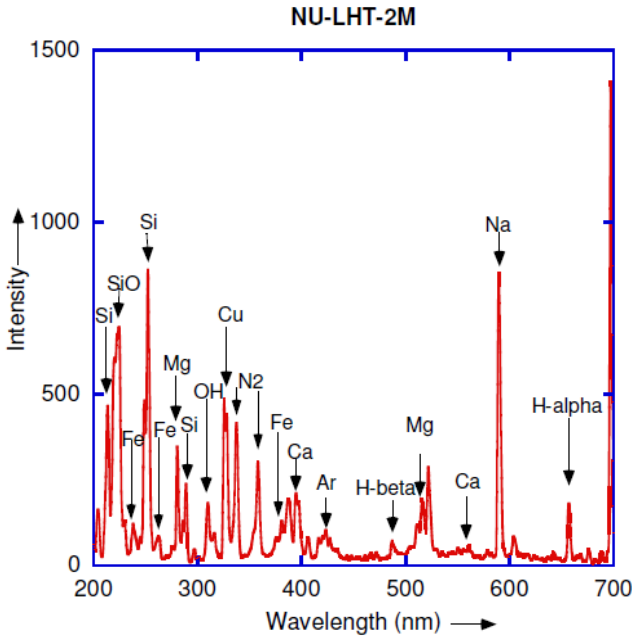

5.1.6: MHCD-OES spectrum of NU-LHT-2M

VII) Ro-Tails:

Ro-Tails, one of the most heterogeneous simulants out of the seven simulants consists of 90% pyroxenes, 5-7% chlorites ($[Mg, Fe]_3 [Si, Al]_4 O_{10} [Mg, Fe]_3 [OH]_6$) and the rest 3-5% comprise impurities. Both clinopyroxene (Ca, Mg, Fe Silicate) and ortho-pyroxene (Fe, Mg silicate) are present with clinopyroxene being the more dominant of the two, leading to a higher concentration of Ca. A small amount of Na is consistent with its presence as an impurity.

RO-Tails composition can be summarized in table 5.1.8 as follows:

Oxides	Wt%
SiO_2	42.62
CaO	15.8
MgO	19.8
Fe_2O_3	21.8

Table 5.1.8: RO-Tails Composition

Out of all the seven samples, RO-Tails has the maximum amount of pyroxene present. That is why the elements, Mg and Fe, which are mostly the constituents of the mineral pyroxene, are present in very high concentrations in RO-Tails. The Ro-Tails spectrum (as shown in figure 5.1.7) obtained using MHCD-OES analysis clearly shows the high-intensity peaks of the Mg and Fe, especially the 239nm and 260nm peaks of iron and 280nm peak of Mg. This once again points towards the analytical utility of the MHCD unit, which can not only detect chemical species but can also track their concentrations in the analyte. Ro-Tails doesnot have a Na bearing mineral. Any Na present in it, therefore, should be present in very low concentration and in the form of impurity. The MHCD-OES device demonstrates its analytical capability by detecting the small amount of Na while at the same time producing a low-intensity spectral line of Na that corresponds to its low concentration in Ro-Tails.

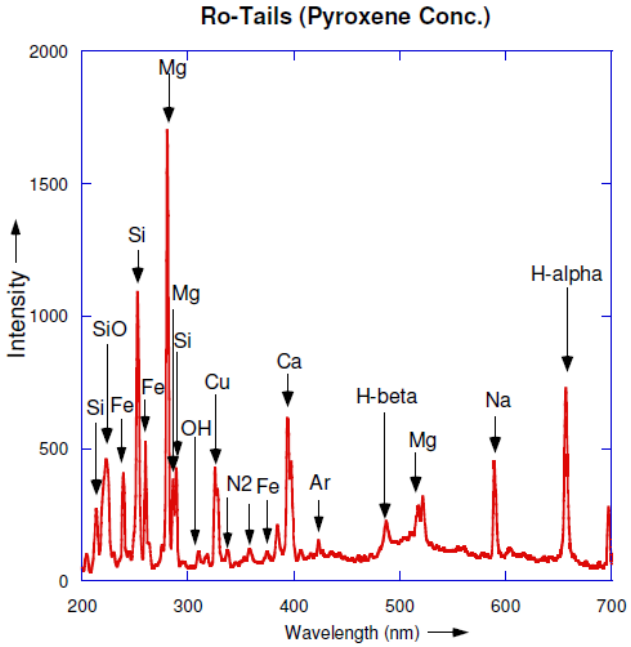

5.1.7: MHCD-OES spectrum of RO-Tails

The summary plot (figure: 5.1.8) compares the spectra of the seven lunar regolith simulants. Simulants in which plagioclase is the main component, e.g. Synthetic Anorthite, CL2.CON, and Chenobi have a Fe emission peak of very low intensity compared to that of the other simulants which have pyroxene as the dominant component. High-intensity emission peaks of Fe can be observed at 239nm in case of JSC-1, JSC-1A and Ro-Tails, indicating the higher concentrations of Fe of 10.79%, 20.67% and 21.8%, respectively present in these simulants. In the case of RO-Tails, the Mg peak at 280nm is very strong, reflecting the high concentration of Mg present in the sample. Synthetic Anorthite and Ro-Tails have a very low concentration of Na, which is present as an impurity in the samples. This fact is well represented in their respective spectra which show the Na line intensity to be the least compared to the OES spectra from the other regolith simulants.

The following summary graph (figure 5.1.8) serves to illustrate the sensitivity of the MHCD-OES technique and its analytical utility by illustrating the differences in the spectra of the seven simulants that have different chemical composition.

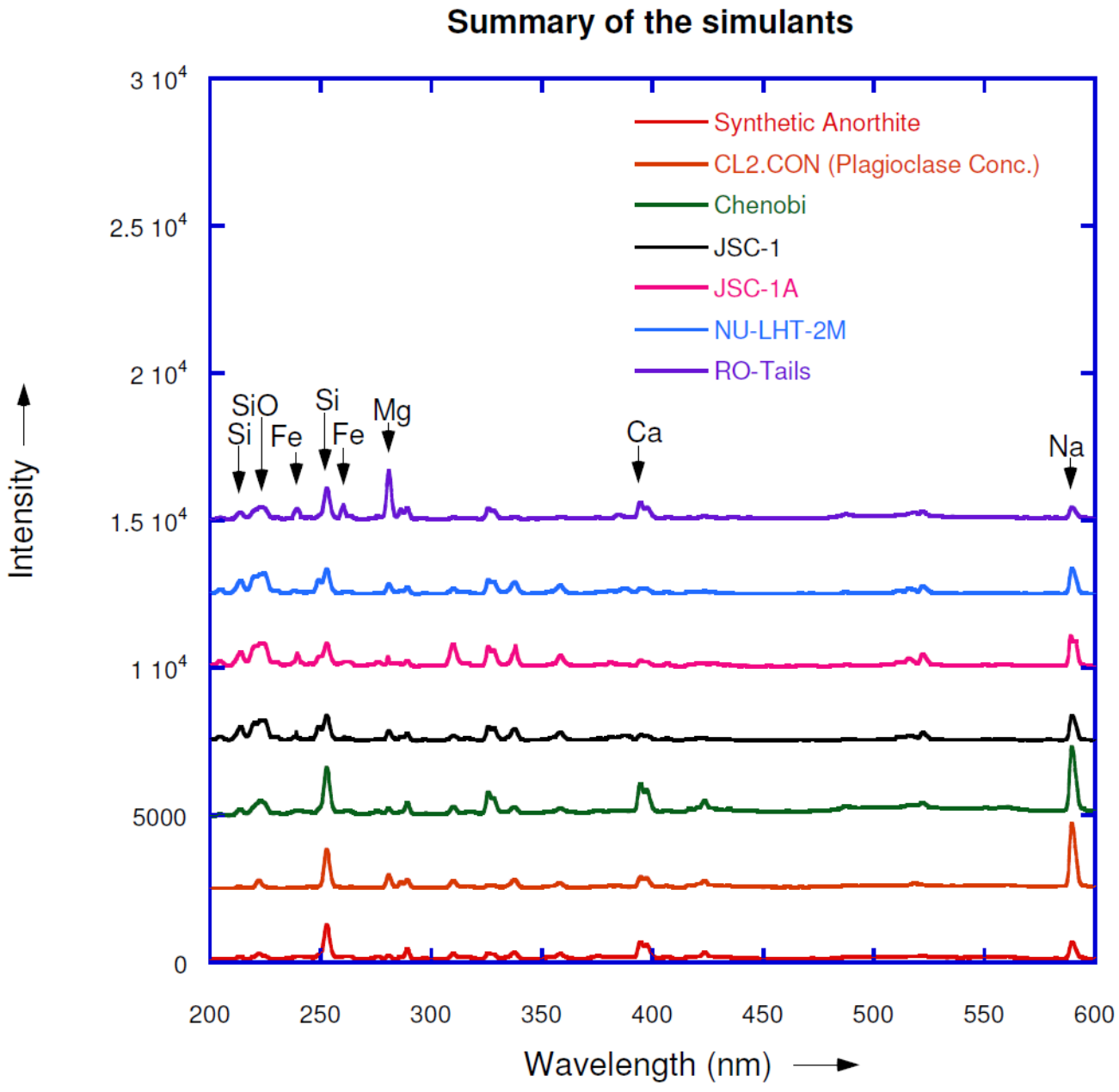

Fig 5.1.8: Summary graph of the seven simulants

5.2 Analytical Precision:

Analytical precision was tested by spectral consistency across time after a given sample charge and also between different sample charges of the same simulant. With the assumption that the plasma action uniformly erodes the particles for a given sample charge, the spectra should contain all lines of associated elements at the same relative intensities. If so, then analytically results will not be biased by sample "age" within the plasma. The observed self-consistency within any given set of spectra for the different simulants gives confidence of the plasma's analytical measure of their elemental composition.

With this analytical precision established, the variability of the plasma with respect to simulant mineral content can also be assessed by testing it against different charges of the same heterogeneous simulant and observing that it produces different spectra with each charge. The heterogeneous simulant used in this case was NU-LHT-2M. Spectra within a series for a given charge of NU-LHT-2M were consistent (as indicated previously), but varied collectively between sample charges. Experimental variability was assessed by repeated measurements using Synthetic Anorthite, a homogeneous simulant. Therefore comparison between spectral sets illustrate that the micro-plasma analysis technique is a consistent elemental analysis technique and can distinguish between minerals present in one simulant.

An averaged spectrum representing a series was calculated for each sample. Three separate series were obtained for each simulant (by analyzing three separate sample charges). To facilitate the calculation of peak intensities from the many spectra, a macro code based on the commercial software Kaleidagraph™ was written. It supplied spectral intensities with a two-point background subtraction. Further details may be found in Appendix A. The spectral intensities thus calculated were plotted as percent relative intensity for each of the three "series spectra", in bar graph format, for the two simulants. Each bar graph compares the relative percentages of elements across the 3 series for each simulant. For the homogenous simulant Synthetic Anorthite, results are consistent, i.e. similar relative intensities are observed for a particular element as measured in separate tests, but not for the heterogeneous simulant NU-LHT-2M.

Synthetic Anorthite:

For a highly uniform sample, such as the Synthetic Anorthite, there should be little difference between spectra for different sample charges. As presented in the bar-graph plot (figure.5.2.1), the averaged relative intensities of any particular element have very little variation over the three series, thereby proving that the data collected using this technique are consistent. Thus it can be concluded that micro-plasma analysis has good analytical precision (consistency). The error bars calculated based on the standard deviation of a series of forty spectra (collected for a sample charge) represent signal variation over a single-sample charge, which is also relatively less indicating the precision of the technique.

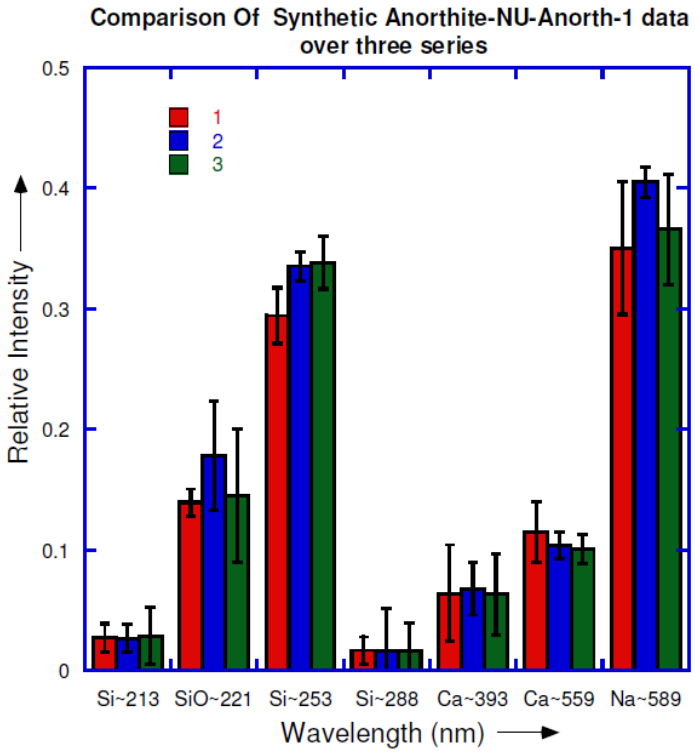

Fig 5.2.1: Comparison of elemental relative peak intensities over three sets of spectral analysis of Synthetic Anorthite

To have a very clear idea about the magnitude of variation of relative intensities for an element over the three series, the deviation (from the mean) of relative intensities is calculated and plotted. The plot in figure 5.2.2 points out that the percentage deviation of averaged relative intensity for any particular wavelength is less than 20%, which is relatively much lesser as compared to the case of NU-LHT-2M (as illustrated later) . Thus it can be concluded that plasma analysis is an analytical technique which yields reproducible data. For a simulant with known uniform composition, the relative percent differences between measurements can then serve as a measure of the relative standard

deviation, i.e. the experimental uncertainty. This measure can be adopted as a metric of the experimental variability.

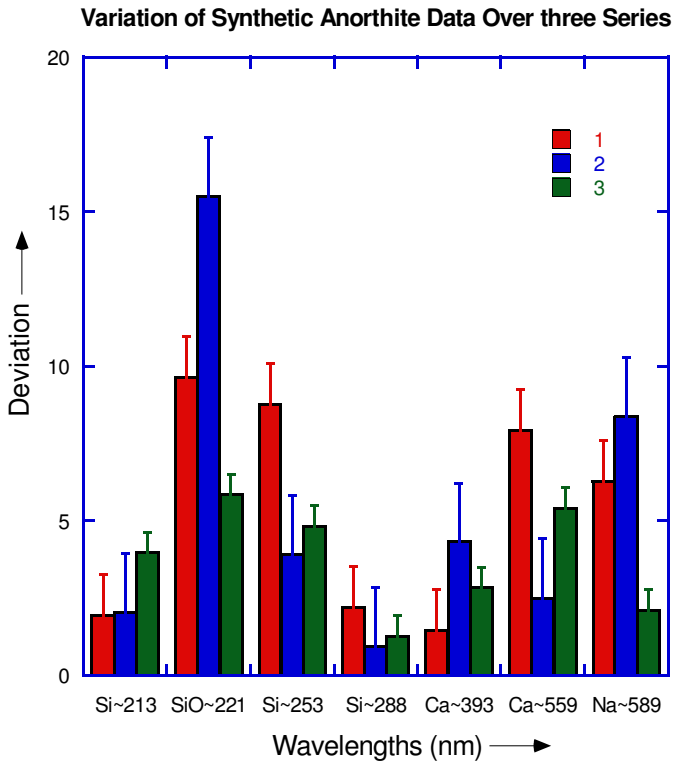

Fig 5.2.2: Variation Of Synthetic Anorthite relative peak intensities over three series

NU-LHT-2M:

The situation is quite different for NU-LHT-2M, a heterogeneous simulant sample. The relative intensities corresponding to any given element concentration are quite divergent between sample charges. This is illustrated by the variation among spectral relative intensities for each observed element as presented in figure.5.2.3 for the three series of data collected.

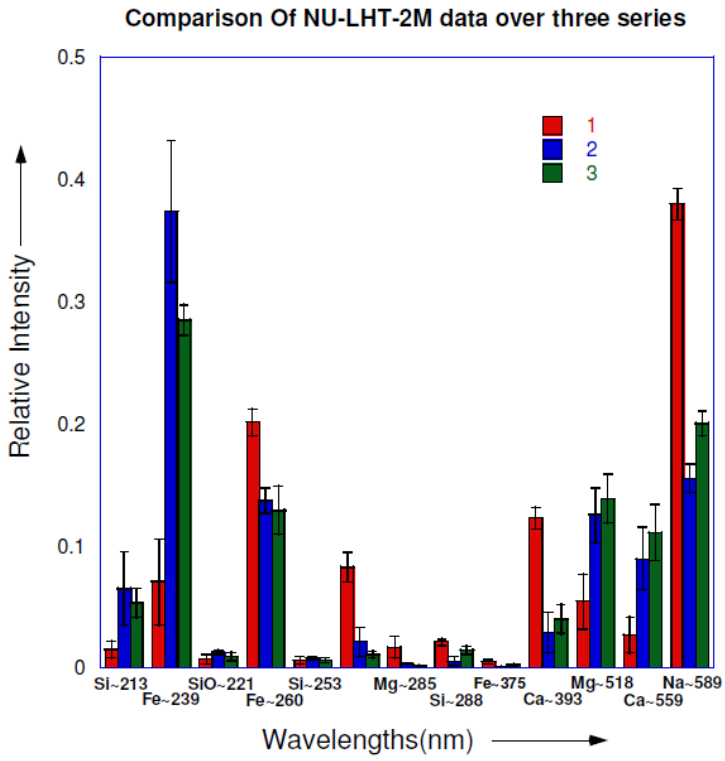

Fig 5.2.3: Comparison of elemental relative peak intensities over three sets of spectral analysis of NU-LHT-2M

The deviations of the relative intensities, from the mean (as calculated from the series) are also plotted and shown in figure. 5.2.4. It can be observed from the plot that the deviations are high (with a maximum of 140%), reflecting mineral heterogeneity. The relative percent differences for the NULHT-2M material for some elements (e.g., Mg, Ca) is quite high (greater than 100%). In contrast much smaller variability is observed for the Si peak at 253nm, but not at all wavelengths. These large differences reflect the mineral variability between sample charges for this mineralogical heterogeneous simulant, and illustrate that micro-plasma analysis has a dynamic range to detect large

variations as well as sufficient sensitivity for smaller compositional differences given its analytical precision.

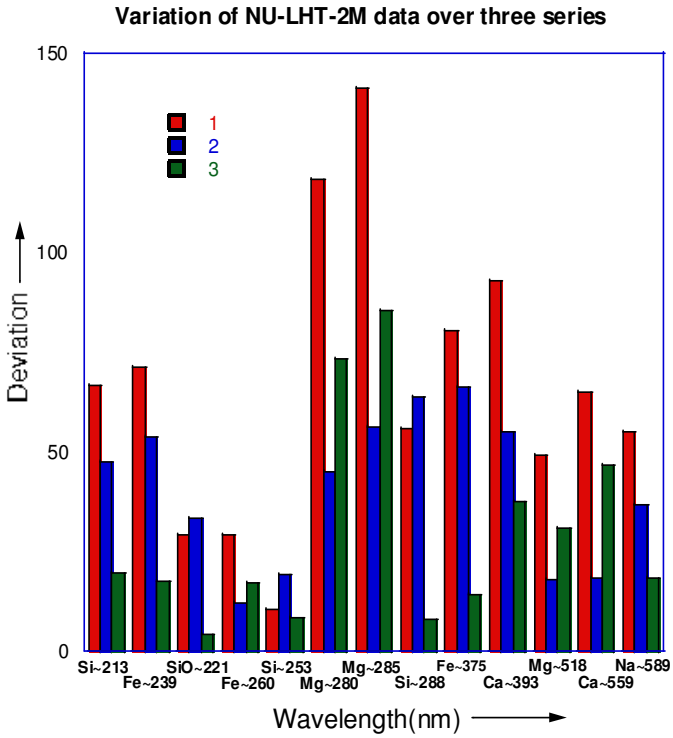

Fig: 5.2.4: Variation Of NU-LHT-2M. peak intensity over three series

5.3 Analytical Accuracy:

Analytical accuracy of the MHCD-OES technique was verified by comparing the MHCD-OES generated results with the reference data. Based on the MHCD-OES generated spectra for different lunar regolith simulants, the relative intensities of the emission lines were calculated. The relative intensity of a peak in a spectrum of a specific sample represents the concentration of the corresponding element in that sample. Therefore the relative intensities calculated for each of the major peaks across the sample spectra of the seven simulants were matched against the reference data.

It was observed that though the percentage composition as calculated by the micro plasma technique did not exactly match the reference values (as expected), the pattern of the values for a particular element across the samples was similar to the pattern of reference values for that same element.

The analyses results illustrated by the bar graph analysis in figure series 5.3.1-5.3.5 compare the experimentally calculated atomic percentage values for the five elements with the corresponding reference values. This analysis was conducted for all the 5 major elements which are present in different proportions in the seven simulant samples.

The experimental results derived by MHCD-OES have many experimental factors that could contribute to differences in comparison to the reference data. First and foremost is that the emission intensity reflects the radiative transition strength. This factor, along with optical collection efficiency (presumably the same for all wavelengths of interest) plus wavelength dependence of detection will cause variance in the observed relative intensities compared to the true elemental contents.

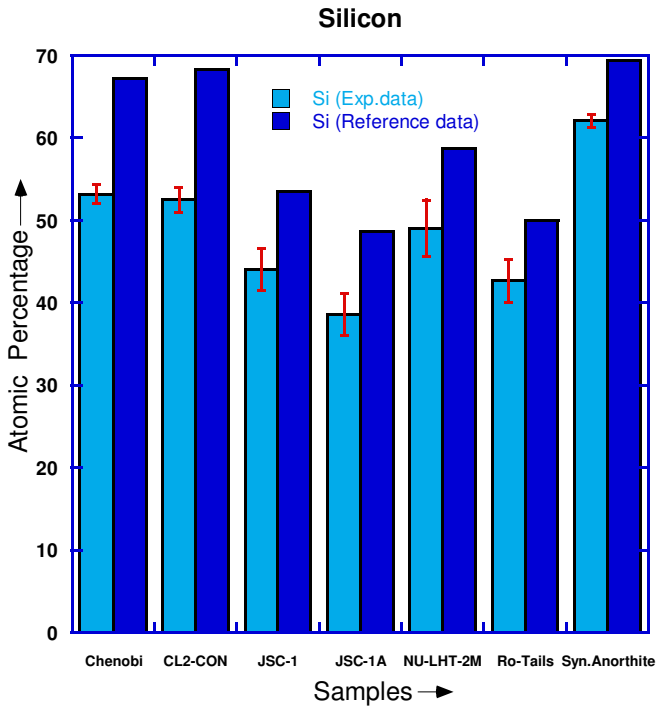

Fig: 5.3.1: Comparison of experimental data with reference data for Si

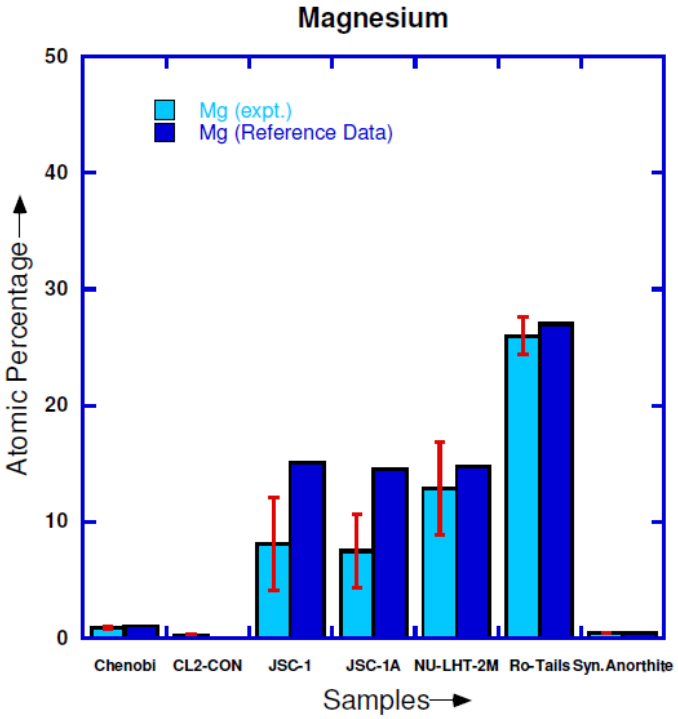

Fig 5.3.2: Comparison of experimental data with reference data for Mg

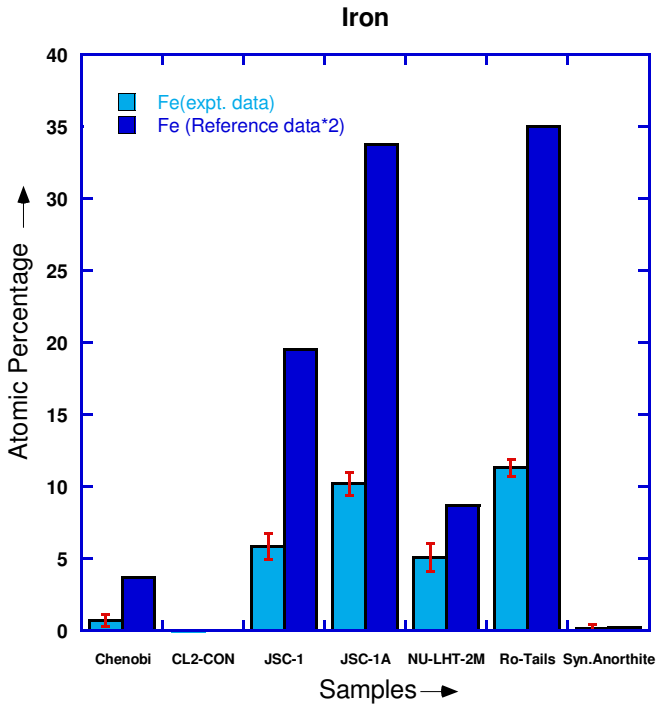

Fig: 5.3.3: Comparison of experimental data with reference data for Fe

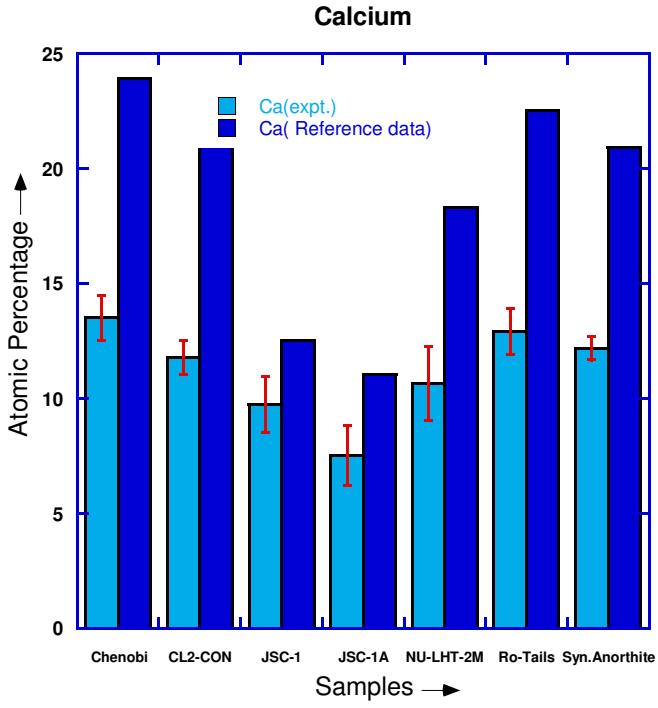

Fig. 5.3.4: Comparison of experimental data with reference data for Ca

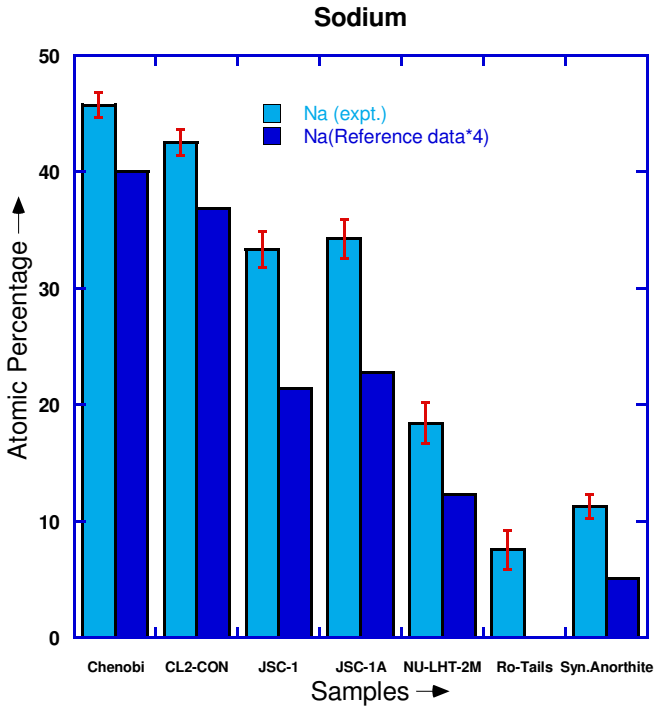

Fig 5.3.5: Comparison of Experimental data with Reference data for Na

5.4. Matrix Effect:

The matrix effect arises because of different crystallography or bonding of the elements of interest within the different mineral components of the simulants. It causes the optical signals generated by MHCD-OES analysis to depend upon the sample structure besides depending on the elemental composition. The scaling factor calculated as the ratio between observed elemental content and the known reference value provides a direct measure of the matrix effect. Basically it encompasses two factor sets–the first includes all instrumental parameters which will normally remain fixed over the course of the measurements and the second factor includes the mineral variation across simulants, which contributes to the matrix effect.

The scaling factor analysis results are plotted for each element, across the different simulant samples in figures 5.4.1-5.4.5. It can be observed from the bar graphs that the scaling factor for a particular element varied across different samples. In other words the normalization for variation in element concentration did not yield a constant value. The scaling factor provides a straight forward statistic of the MHCD's analytical ability. If a database can be developed with the common lunar regolith simulants, their composition and appropriate element-specific scaling factors, MHCD-OES could be calibrated to identify directly any unknown simulant and thus can be developed (beyond elemental analysis) into an in-situ MHCD analytical instrument for analysis of lunar mineralogy.

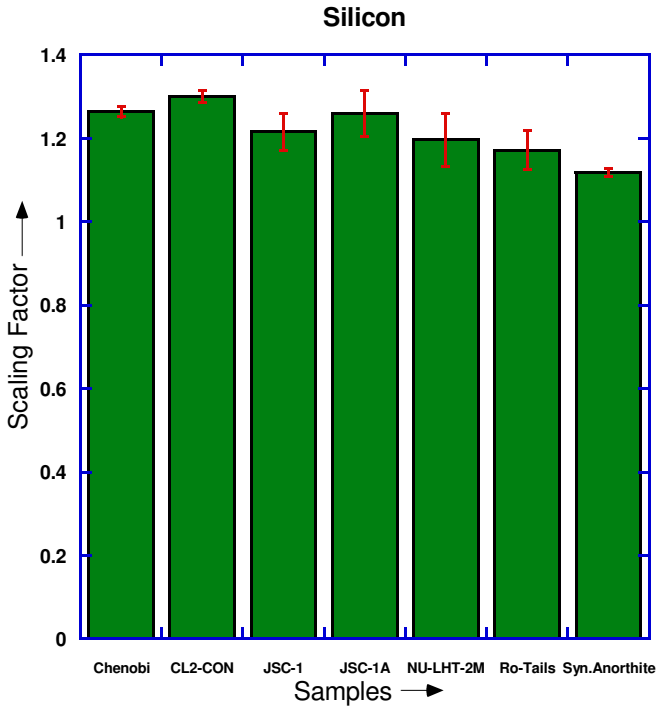

Fig 5.4.1: Scaling Factors across Samples

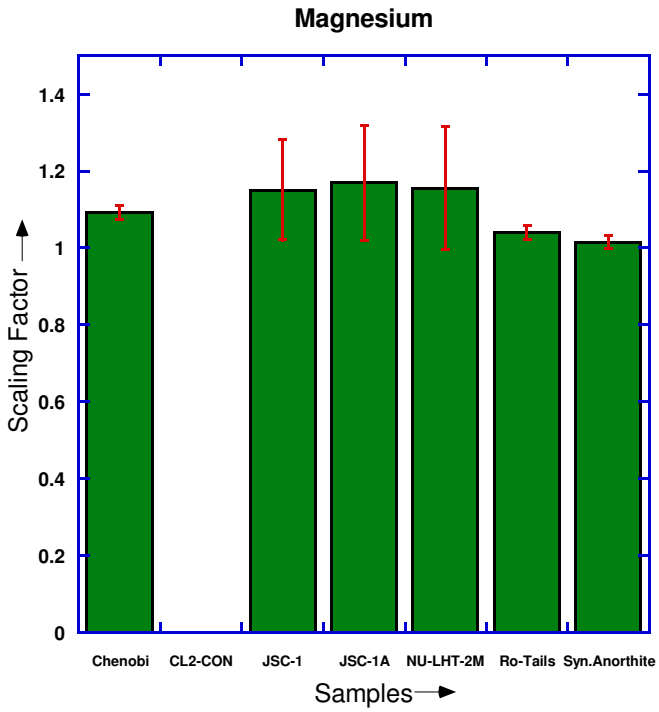

Fig 5.4.2: Scaling Factors across Samples

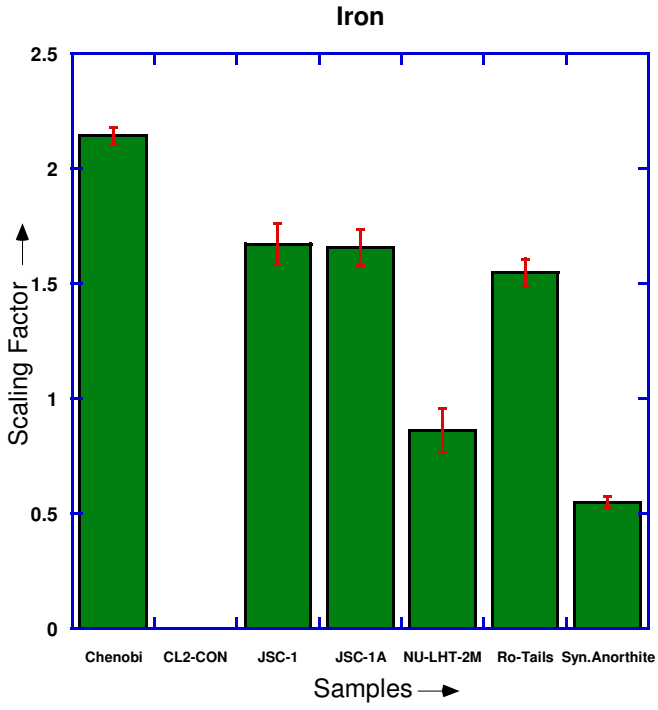

Fig 5.4.3: Scaling Factors across Samples

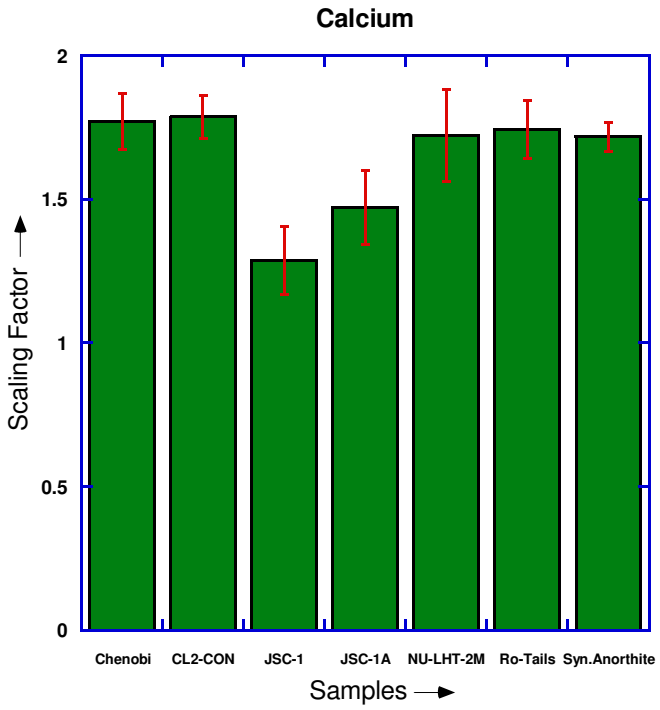

Fig 5.4.4: Scaling Factors across Samples

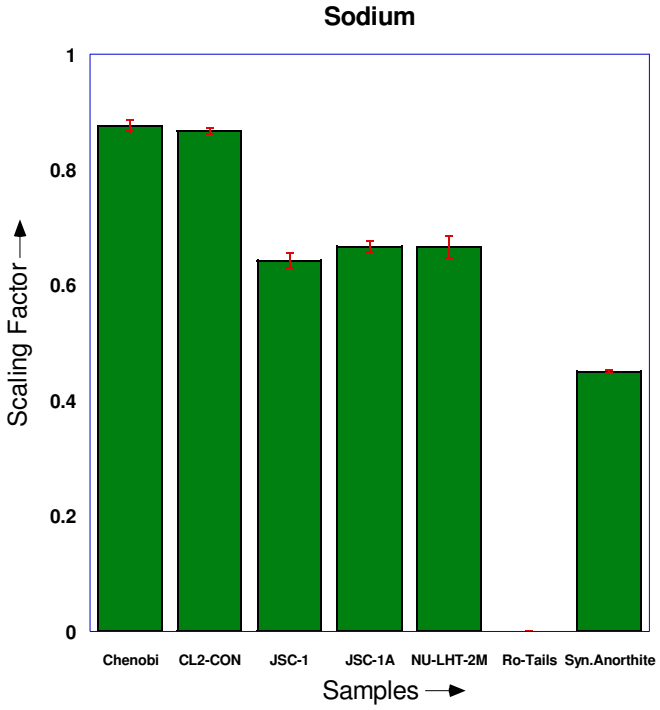

Fig 5.4.5: Scaling Factors across Samples

5.5. Dynamic Range and Linearity:

To clearly compare MHCD-OES intensity with elemental concentration, plotted in figure set 5.5.1-5.5.5 are the observed emission intensities of the elements of interest versus their respective concentration ranges across the simulants. By so separating element-specific signals, analytic range and linearity can be directly evaluated. The plots show signal variation across the elemental concentration range for the five major elements present in the lunar simulants. Error bars were calculated based on the standard deviation for a set of 200 independent spectra. The linear curve set was evaluated based on minimizing the usual sum of least squares, i.e residuals.

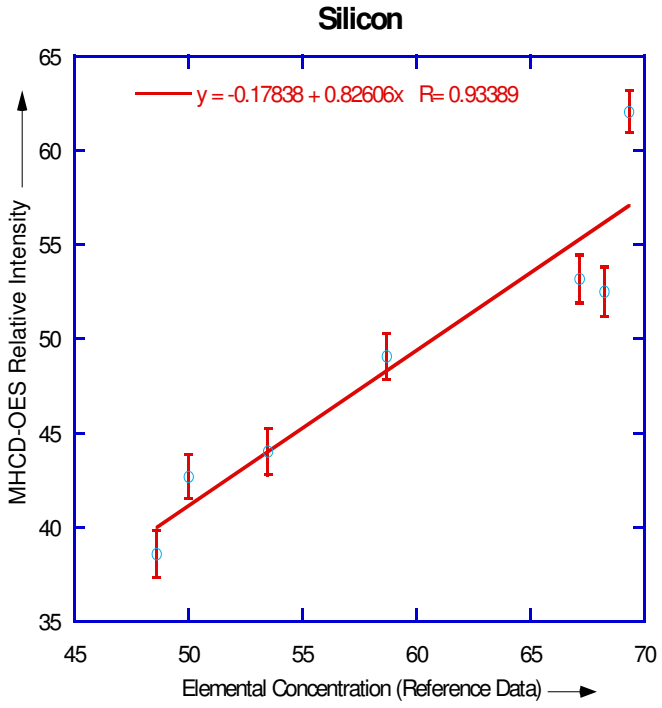

Fig.5.5.1: Signal Variation with Elemental Concentration

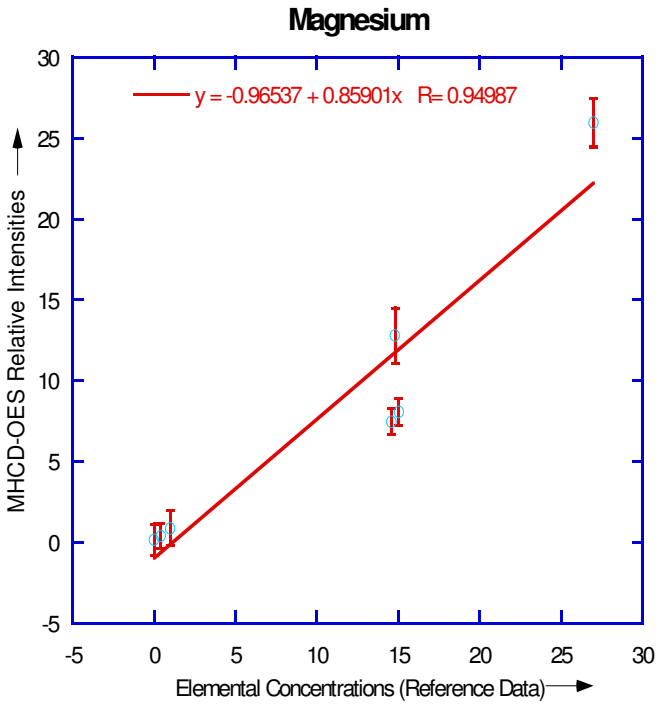

Fig.5.5.2: Signal Variation with Elemental Concentration

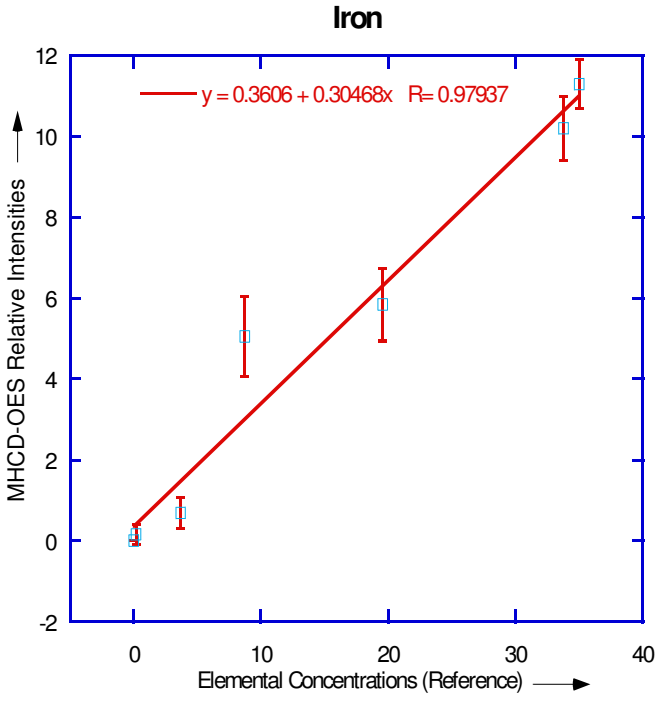

Fig.5.5.3: Signal Variation with Elemental Concentration

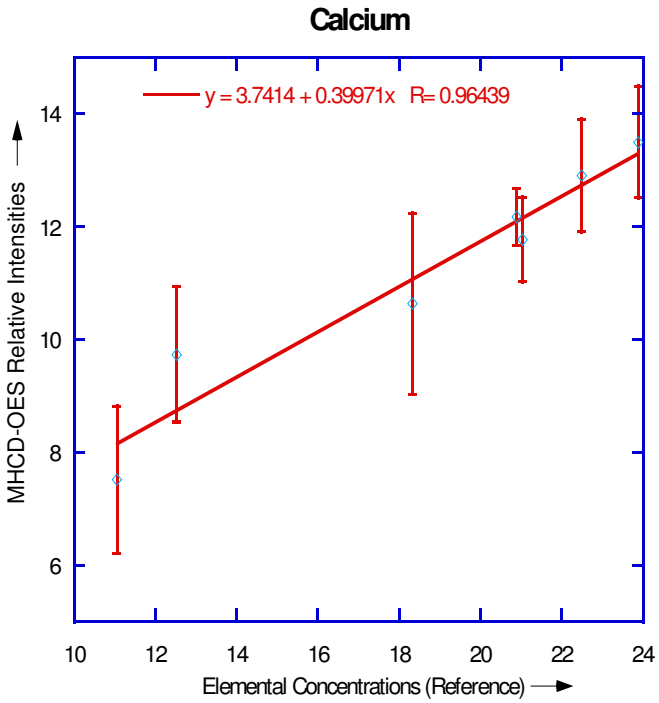

Fig.5.5.4: Signal Variation with Elemental Concentration

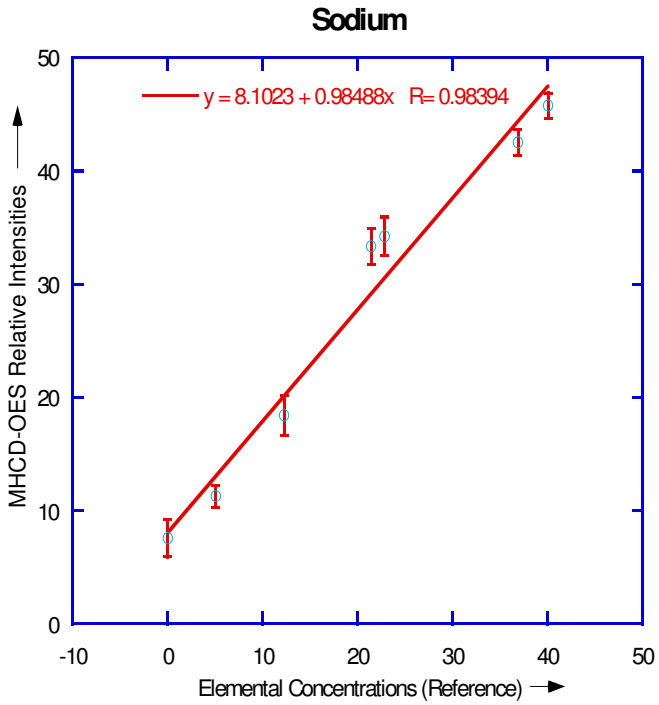

Fig.5.5.5: Signal Variation with Elemental Concentration

Based on the correlation coefficients calculated for each element, it can be concluded that a linear response exist between the signals obtained from the MHCD-OES analysis and the elemental concentrations for each element. Therefore, OES signals as a function of specific element concentrations across the range of minerals (simulants) tested could be directly evaluated. Such signal versus concentration analysis constitutes the normal analytical curves for illustrating technique/instrument linearity and dynamic range.

5.6 Summary:

This chapter illustrates the analytical utility of the micro-hollow plasma analysis as an effective and sensitive tool in the analysis of lunar regolith simulants. Using the seven lunar regolith simulant samples the basic figures of merits were tested, which includes elemental detection and concentration, linearity and dynamic range and sensitivity of the technique to matrix effect. The two key parameters, precision and accuracy, which are essential to assessing the above-mentioned figures of merits, were also tested.

Chapter 6

CONCLUSIONS AND RECOMMENDATIONS FOR FUTURE WORK

6.1. Conclusions:

Micro-Hollow Cathode Discharge (MHCD) is a novel technique for the analysis of lunar regolith simulants. This work develops MHCD-OES as an alternative technique to LIBS (Laser Induced Breakdown Spectroscopy) for the compositional analysis of the lunar regolith simulants.

As outlined in the Results chapter the MHCD-OES technique's precision was tested as experimental variability. With the precision of the technique established the signal variation of MHCD-OES with different charges of the heterogeneous lunar simulant NU-LHT-2M was observed, indicating the signal dependence on mineral content.

Accuracy of the technique was gauged by comparison of the MHCD-OES analysis results to the known elemental compositions of the simulants, as provided by an independent analysis technique. Though the percentage composition as calculated by the MHCD-OES tool did not exactly match the reference values (as expected), the pattern of the values for a particular element across the samples was similar to the pattern of reference values for that same element. To correct for such variations scaling factors were calculated as the ratio between observed MHCD-OES signal and the known reference value. Scaling factors encompass both instrumental response and mineral variation in the different simulants, the later giving rise to the matrix effect. Linearity and dynamic range testing

are set by the simulants tested. The elemental range and technique linearity evaluation within this range were preset by the concentration range of that element across the simulants. Based on the correlation coefficient calculated from such analysis it can be inferred that the MHCD-OES generated signals have a linear response to elemental concentration, thereby simplifying interpretation of the signal levels.

Finally testing simulants with actual minerals permits insight into potential matrix effects. Matrix effects allow mineral-specific elemental detection wherein analysis results also depend upon sample structure and not solely upon elemental composition. In the context of a limited set of minerals (with known composition) such dependence could be an advantage towards identification of minerals or distinguishing minerals with similar composition, particularly when coupled with MHCD's utility to analyze small quantities (10'sμg). But further work would be required to test whether such variability can be traced to mineral content. Ideally each spectrum could then be represented as a linear summation of mineral specific spectra. With MHCD-OES particle to particle mineral assessment is also a potential capability.

The other important feature that makes MHCD-OES a unique analytical technique is its capability to generate a high S/N ratio, greater than 100, using only 1μg of sample for analyses. Moreover the small size of the device as compared to the size of its equivalent analytical equipment such as ICP-OES or LIBS makes it highly portable and therefore applicable for in-situ operations in space for lunar soil analysis. Its simple construction,

low power consumption and operational simplicity make it a very low-cost device ideal for real-time analyses.

To test the applicability of the MHCD-OES technique for analysis of other solid samples, experiments were also conducted using carbonaceous materials in the form of soots produced by burning materials. The results of soot sample analysis (included in Appendix B) using MHCD-OES confirm that MHCD-OES can be used for analysis of other solid samples as well.

6.2. Recommendations:

A database prepared with the common lunar regolith simulants, their composition and appropriate element-specific scaling factors, would add great value to the MHCD-OES device. Using this database MHCD-OES could be calibrated to identify directly any unknown simulant and thus could be developed (beyond elemental analysis) into an in-situ MHCD analytical instrument for analysis of lunar mineralogy.

This technique should be further tested against other pure compounds (which would not demonstrate matrix effects) to study if the relative intensities as obtained by the MHCD-OES analysis match the corresponding elemental concentrations. In these cases, since the compounds do not demonstrate the matrix effect, even if a scaling factor is required to encompass the instrumental variations, it should remain constant for an element across all such samples, thereby enabling the detector to directly determine the composition of a broader array of samples. Further studies can also be done to investigate the limit of

detection (LOD) for each element. All such tests would enable MHCD-OES to be established as an analytical device for in-situ analyses of a variety of solid samples.

Bibliography

1. Boumans, P. W. J. M., Inductively Coupled Plasma Emission Spectroscopy. *John Wiley and Sons* **1987**.

2. Lochte-Holtgreven, W., Plasma Diagonistics,North-Holland,Amsterdam. **1968**.

3. Eden, J. G.; Park.S.J.; Ostrom, N. P.; Chen.K.F., Recent advances in microcavity plasma devices and arrays: a versatile photonic platform. *Journal of Applied Physics D: Applied Physics* **2005,** *38* (1644-1648).

4. Schoenbach, K. H.; Verhappen, R.; Tessnow, T.; Peterkin, F. E., Microhollow cathode discharges. *Applied Physics Letters* **1996,** *68* (1), 13-15.

5. White, A. D., New Hollow Cathode Discharge. *Journal of Applied Physics D: Applied Physics 30*, 711-719.

6. El-Habachi, A.; schoenbach, K. H., Emission of excimer radiation from direct current,high pressure hollow cathode discharges. *Applied Physics Letters* **1998,** *72*, 22-24.

7. Broekaert, J. A. C., The development of microplasmas for spectrochemical analysis. *Analytical and Bioanalytical Chemistry* **2002,** *374*, 182-187.

8. Sakai, O.; Hashimoto, S.; Hatango, A., Switching and regulation of a pulsed discharge channel in a coplanar plasma tetrode. *Applied Physics Letters* **2003,** *82* (15), 2392-2395.

9. Moselhy, M. M.; Shi, W.; Stark, R. H.; Schoenbach, K. H., Xenon excimer emission from pulsed microhollow cathode discharges. *Applied Physics Letters* **2001,** *79* (9), 1240-1243.

10. Radziemski, L.; Cremers, D.; Benelli, K.; Khoo, C.; Harris, R. D., Use of the vacuum ultraviolet spectral region for LIBS-based Martian geology and exploration. *Spectrochimica Acta Part B* **2005,** *60*, 237-248.

11. Wiggins, D. L.; Raynor, C. T.; Johnson, J. A., Evidence of inverse bremsstrahlung in laser enhanced laser-induced plasma. *American Institute of Physics* **2010,** *17* (10).

12. http://unicorn.ps.uci.edu/H2A/handouts/PDFs/RWFRover.pdf.

13. http://mpfwww.jpl.nasa.gov/MPF/mpf/sci_desc.html.

14. Tendero, C.; Tixier, C.; Tristant, P.; Desmaison, J.; Leprince, P., Atmospheric pressure plasmas: A review. *Spectrochimica Acta Part B: Atomic Spectroscopy* **2006,** *61*, 2-30.

15. Barankova, H.; Bardos, L., Atmospheric Pressure Plasma Sources and Processing. *Handbook of Deposition Technologies for Films and Coatings (Third Edition) — Science, Applications and Technology* **2010**, 865-880.

16. Nehra, V.; Kumar, A.; Dwivedi, H. K., Atmospheric Non-Thermal Plasma Sources. *International Journal of Engineering* **2008,** *2* (1), 53-68.

17. Chirokov, A. V., Stability of Atmospheric Pressure Glow Discharges. *Phd. Thesis Drexel University* **2005**.

18. Longwitz, R. G.; Lintel, H. V.; Renaud, P., Study of micro-glow discharges as ion sources for ion mobility spectrometry. *Journal of vacuum science and technology B* **2003,** *21* (4).

19. Tachibana, K., Current Status of Microplasma Research. *Transactions on Electrical and Electronic Engineering* **2006,** *1* (2), 145-155.

20. Becker, K.; Schoenbach, K. H.; Eden, J. G., Microplasmas and applications. *Journal of Physics D: Applied Physics* **2006,** *39*, R55-R70.

21. Schoenbach, K. H.; Moselhy, M. M.; Shi, W.; Bentley, R., Microhollow cathode discharges. *Journal of Vacuum science and technology A* **2003,** *21* (4), 1260-1265.

22. Machala, Z.; Marode, E.; Laux, C. O.; Kruger, C., DC Glow Discharges in Atmospheric Pressure Air. *Journal of advanced oxidation technologies* **2004,** *7* (2), 133-137.

23. Miclea, M.; Kunze, K.; Heitmann, U.; Florek, S.; Franzke, J.; Niemax, K., Diagnostics and application of the microhollow cathode discharge as an analytical plasma. *Journal of Physics D: Applied Physics* **2005,** *38* (11), 1709-1715.

24. Baars-Hibbe, L.; Sichlerb, P.; Schradera, C.; Geßnera, C.; Gericke, K. H.; Bu¨ttgenbach.S., Micro-structured electrode arrays: atmospheric pressure plasma processes and applications. *Surface and Coatings Technology* **2003,** *174*, 519-523.

25. Karanassios, V., Microplasmas for chemical analysis: analytical tools or research toys? *Spectrochimica Acta Part B: Atomic Spectroscopy* **2004,** *59* (7), 909-928.

26. Schoenbach, K. H.; El-Habachi, A.; Moselhy, M. M.; Shi, W.; Stark, R. H., Microhollow cathode discharge excimer lamps. *Physics of Plasmas* **2000,** *7* (5), 2186.

27. Miclea, M.; Kunze, K.; Franzke, J.; Niemax, K., Plasmas for lab-on-the-chip applications. *Spectrochimica Acta Part B: Atomic Spectroscopy* **2002,** *57*, 1585-1592.

28. Miclea, M.; Okruss, M.; Kunze, K.; Ahlman, N.; Franzke, J., Microplasma-based atomic emission detectors for gas chromatography. *Analytical and Bioanalytical Chemistry* **2007,** *388*, 1565-1572.

29. Miclea, M.; Kunze, K.; Franzke, J.; Niemax, K., Microplasma jet mass spectrometry of halogenated organic compounds. *Journal of Analytical Atomic Spectrometry* **2004,** *19*, 990-994.

30. http://www.stellarnet-inc.com/Pressrel_BLACK-Comet-HR%20high%20resolution%20concave%20grating%20spectrometer.htm.

31. Granier, A.; Vervloet, M.; Aumaille, K.; Vallee, C., Optical emission spectra of TEOS and HMDSO derived plasmas used for thin film deposition. *Plasma Sources Science Technology* **2003,** *12*, 89-96.

32. Conte, R. A.; VanVeen, E. H.; DeLoos-Vollebregt, Fast survey analysis of biomass by-product samples based on ICP optical emission spectra. *Journal of Analytical Chemistry* **1999,** *364*, 666-672.

33. Hosseinimakarem, Z.; Tavassoli, H. S., Analysis of human nails by laser-induced breakdown spectroscopy. *Journal of Biomedical Optics* **2011,** *16*.

34. Essington, M. E.; Melnichenko, G. V.; Stewart, M. A.; Hull, R. A., Soil Metals Analysis Using Laser-Induced Breakdown Spectroscopy (LIBS). *Soil Science Society of America Journal* **2009,** *73*.

35. Chenglong, Y.; Zhuang, Z.; Tu, Y.; Yang, P.; Wang, X., Thermospray nebulizer as sample introduction technique for microwave plasma torch atomic emission spectrometry1. *Spectrochimica Acta Part B* **1998,** *53*, 1427-1435.

36. Phillips, B. L.; Kirkpatrick, R. J., Investigation of short-range Alosi order in synthetic anorthite by ^{29}Si MAS NMR spectroscopy. *American Mineralogist* **1992,** *77*, 484-494.

37. http://www.evcltd.com/index_005.htm.

38. McKay, D. S.; Carter, J. L.; Boles, W. W.; Allen, C. C.; Allton, J. H. JSC-1: A NEW LUNAR SOIL SIMULANT *American Society of Civil Engineers* [Online], 1994, p. 857-866.

39. http://www.orbitec.com/store/JSC-1A_Bulk_Data_Characterization.pdf.

40. Wilson, S.; Stoeser, D.; Rickman, D. Design and Specifications for the Highland Regolith Prototype Simulants NU-LHT-1M

and -2M 2010.

41. Ruff, G. A.; Urban, D. L., Technology development for fire safety in exploration spacecraft and habitats. In *45th AIAA Aerospace Sciences Meeting and Exhibit,AIAA 2007-350*, 2007; pp 1-14.

42. Mulville, D. R. In *Flammability,Odor,Offgassing and Compatibility Requirements and Test Procedure for Materials in Environments that support combustion, NASA-STD-6001,*1998.

43. http://www.oceanoptics.com/Products/maya.asp.

44. Acquaviva, S.; Giorgi, M. L., High-resolution investigations of C2 and CN optical emissions in laser-induced plasmas during graphite ablation. *Journal of Physics B:Atomic,Molecular and optical Physics* **2002,** *35* (4), 795-802.

45. Rohlfing, E. A., Optical emission studies of atomic, molecular, and particulate carbon produced from a laser vaporization cluster source. *Journal of Chemical Physics* **1988,** *89* (10), 6103-6113.

46. Nemes, L.; Keszler, A. M.; Hornkohl, J. O.; Parigger, C. G., Laser-induced carbon plasma emission spectroscopic measurements on solid targets and in gas-phase optical breakdown. *Applied Optics* **2005,** *44* (18), 3661-7.

47. Fernandez, P. C. Fires in Spacecraft.

48. http://www.dura-foam.com/resources/foam-roofing/nasa-shuttle-fuel-tank/.

49. Zhu, X.-M.; Pu, Y.-K., Optical emission spectroscopy in low-temperature plasmas containing argon and nitrogen: determination of the electron temperature and density by the line-ratio method. *Journal of Physics D: Applied Physics* **2010,** *43* (40), 1-24.

50. http://en.wikipedia.org/wiki/Kapton.

51. Groh, H. C. D.; Daniels, C. C.; Miller, S. K.; Dever, J. A.; Waters, D. Space Environment Effects on Silicone Seal Materials 2010.

52. Kleiman, J. I.; Tennyson, R. C., Protection of Space Materials From Space Environment. In *Space Technology Proceedings* [Online] 2001.

53. http://www.mindfully.org/Plastic/Teflon/Teflon-HistoryDuPont.htm.

Appendix A

Calculation of Integrated Intensity Data

The following Kaleidagraph program was used to generate the integrated intensity data.

The Kaleidagraph Program:

cell(87,3)=csum([72:89,2:2]); <Calculate Si~213>

cell(88,3)=((cell(72,2)+cell(89,2))/2)*18;

cell(89,3)=cell(87,3)-cell(88,3);

cell(126,3)=csum([90:128,2:2]);< Calculate SiO~221>

cell(127,3)=((cell(90,2)+cell(128,2))/2)*39;

cell(128,3)=cell(126,3)-cell(127,3);

cell(161,3)=csum([129:163,2:2]);<Calculate Fe~239>

cell(162,3)=((cell(129,2)+cell(163,2))/2)*35;

cell(163,3)=cell(161,3)-cell(162,3);

cell(189,3)=csum([164:191,2:2]);<Calculate Si~252>

cell(190,3)=((cell(164,2)+cell(191,2))/2)*28;

cell(191,3)=cell(189,3)-cell(190,3);

cell(212,3)=csum([192:214,2:2]);<Calculate Fe~260>

cell(213,3)=((cell(192,2)+cell(214,2))/2)*23;

cell(214,3)=cell(212,3)-cell(213,3);

cell(256,3)=csum([245:258,2:2]);<Mg~280>

cell(257,3)=((cell(245,2)+cell(258,2))/2)*14;

cell(258,3)=cell(256,3)-cell(257,3);

cell(264,3)=csum([259:266,2:2]);<Mg~285>

cell(265,3)=((cell(259,2)+cell(266,2))/2)*8;

cell(266,3)=cell(264,3)-cell(265,3);

cell(275,3)=csum([267:277,2:2]);<Si~288>

cell(276,3)=((cell(267,2)+cell(277,2))/2)*11;

cell(277,3)=cell(275,3)-cell(276,3);

cell(504,3)=csum([479:506,2:2]);<Fe~375>

cell(505,3)=((cell(479,2)+cell(506,2))/2)*28;

cell(506,3)=cell(504,3)-cell(505,3);

cell(569,3)=csum([535:571,2:2]);<Ca~393>

cell(570,3)=((cell(535,2)+cell(571,2))/2)*37;

cell(571,3)=cell(569,3)-cell(570,3);

cell(899,3)=csum([884:901,2:2]);<Mg~518>

cell(900,3)=((cell(884,2)+cell(901,2))/2)*18;

cell(901,3)=cell(899,3)-cell(900,3);

cell(1058,3)=csum([1003:1060,2:2]);<Ca~559>

cell(1059,3)=((cell(1003,2)+cell(1060,2))/2)*58;

cell(1060,3)=cell(1058,3)-cell(1059,3);

cell(1136,3)=csum([1100:1138,2:2]);<Na~589>

cell(1137,3)=((cell(1100,2)+cell(1138,2))/2)*39;

cell(1138,3)=cell(1136,3)-cell(1137,3);

cell(2052,3)=cell(89,3)+cell(128,3)+cell(163,3)+cell(191,3)+cell(214,3)+cell(258,3)+cell

(266,3)+cell(277,3)+cell(506,3)+cell(571,3)+cell(901,3)+cell(1060,3)+cell(1138,3);

cell(2053,3)=((cell(89,3)+cell(128,3)+cell(191,3)+cell(277,3))/cell(2052,3))*100;

cell(2054,3)=((cell(571,3)+cell(1060,3))/cell(2052,3))*100;

cell(2055,3)=((cell(163,3)+cell(214,3)+cell(506,3))/cell(2052,3))*100;

cell(2056,3)=((cell(258,3)+cell(266,3)+cell(901,3))/cell(2052,3))*100;

cell(2057,3)=(cell(1138,3)/cell(2052,3))*100;

Appendix B

Micro-Hollow Cathode Discharge Analysis of Soot Sample

During the work with Lunar Regolith Simulants a different opportunity arose to further test the Micro-hollow glow discharge (MHCD) analytical capability, but now for an organic material in the form of soots, more generally fire by-products that could be admixtures of soot and inorganic elements. Such interest and need arose from NASA for fire protection in space environments (part of the FPDS program). NASA has needs in its Fire Safety Programs for better fire sensors. To-date around 20 fires have occurred on the space shuttle, all detected by astronauts[41].

Two types of fire sensors such as the ionization and obscuration are used on the space shuttle and space station, for NASA. Both types have recognized limitations in a normal gravity environment and are severely hindered in performance by low gravity's effect upon fires and flames. These not only suffer from a lack of sensitivity but also from false alarms due to triggering of the detector by ambient dust and detritus. Fires in 0 gravity environment are notoriously more difficult to detect. Fundamental studies have shown numerous variations in soot particle concentration, size and yield in 0 gravity (g) environment compared to 1g environment. Therein a more sensitive yet versatile detector is required to surmount such wide parameters. Moreover material combustion is entirely different in terms of both mechanism and reaction products compared to simple laboratory flames. A complex array of physical and chemical processes tends to support gas phase flame. Therein lies the opportunity for a MHCD based fire detector. Materials

by their composition will produce different byproducts and concentrations, most likely of stable end products. Beyond 'sample' detection, identification of multiple fire species would be the basis for a so-called 'smart detector'. Multi species recognition could be used to identify the burning material and hence locate the source of the fire.

Based on the analytical utility of the MHCD device, it was tested as a 'smart fire detector' for its capabilities of detecting fire from burning and pyrolyzing materials, determining C/H elemental ratio of carbonaceous aerosols and distinguishing the combustion produced emissions from ambient inorganic aerosols. This chapter illustrates the results obtained from MHCD analyses of soot samples generated by the combustion or pyrolysis of materials that are presently accepted for use in space exploration (based on NASA standard)[42].

Chapter Outline:

B.1.Experimental Procedure

B.2.MHCD-OES spectra of soot samples

B.3. Analysis of the MHCD-OES spectra for distinctiveness

B.4. C/H Ratio calculation of model compounds

B.5. MHCD-OES analysis of inorganic samples

B.6. Summary

B.1.Experimental Procedure:

The soot samples for the experiments were produced by combustion of six materials approved for use aboard spacecraft. Two of those materials were also pyrolyzed for the C/H analysis. The combustion and pyrolysis were carried out in a combustion system which consists of a 1kW tubular electric furnace mounted vertically and fitted with a quartz tube of 2-inch outer diameter, 1/8-inch wall thickness, and 22-inch length as shown in the fig. B.1.1.

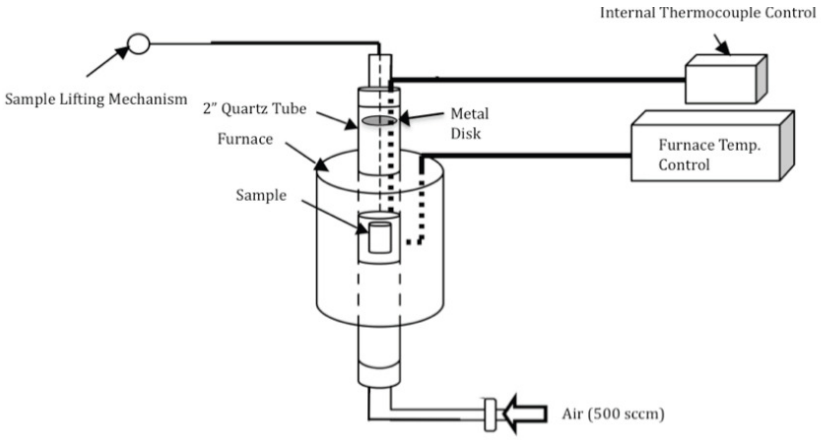

Fig B.1.1.Schematic of the Combustion system

The furnace is equipped with a temperature controller with a controllable temperature up to 1200ºC. The quartz tube is connected to different gas lines. The sample mass varied, depending on the particulate yield from the material. The combustion tests for all samples were performed at 1000 ^{0}C with an air flow of 150 sccm, upwards. Soot and condensable were collected on a copper disk of 0.127 mm thickness. Materials evaluated included polypropylene pellets, polyurethane foam, silicone rubber, Kapton sheet, Teflon and Halar wire insulations that conform to current NASA flammability standards as outlined in by the 6001D Materials Outgasing and Flammability test. Pyrolysis was also carried

out using the same system, but at temperatures of 500 ^{0}C and 900 ^{0}C, using inert gas Helium (instead of air) blown upwards into the vertical furnace system at a flow-rate of 50 SCCM. The soot particulates thus generated served as samples for analyses using MHCD-OES system, discussed later in this chapter.

The MHCD element used for the soot sample analysis (as shown in figB.1.2) was slightly different from that of those used for the lunar simulants. A metalized disk element was prepared by a screen printing process starting with nickel paste films supported on an insulating alumina disc (with laser drilled hole) that were fired, together as a unit. The alumina disc thickness was 250 μm and the hole diameter was 300 μm.

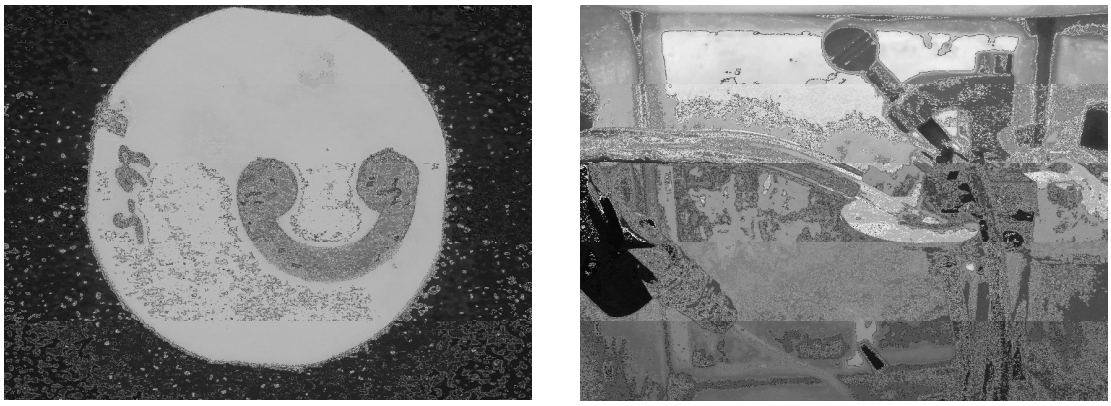

Fig: B.1.2: (a) Metalized disc element (b) metalized disc/Cu disc assembly for experimentation

The MHCD element was assembled with a removable copper disk (backing plate), upon which the sample was collected. The micro-plasma generated between the annulus of the metalized disc serving as anode and cathode sputters the sample contained within the annulus, thus providing for sample analysis.

Spectrometer:

In this case an Ocean Optics Maya2000 Pro Spectrometer was used. This spectrometer is based on an f/4 (101.6 mm), symmetrical, crossed Czerny-Turner design[43]. It uses a scientific grade, back thinned, Hamamatsu S10420 CCD array detector which results in a compact, flexible system, with no moving parts, that's easily integrated as an OEM component. The detector has a total number of 2048 x 64 pixels. The signal to noise ratio of the spectrometer is 450:1 with a dark noise of 8.2 counts, RMS. The power required for its operation is 500 mA at 5VDC. Maya is a microcontroller-controlled spectrometer, thus all operating parameters are implemented through software interfacing to the unit.

The detector covers a wavelength range of 165 – 1100 nm with selectable integration time ranging from 6 ms to 5 seconds. It has a peak quantum efficiency of 75% with a sensitivity of .32 counts per electron and an optical resolution of .75nm. It has a small size of 6 x 4 x 2 inches and a very low weight of 2 lb which makes the system easily portable. This spectrometer was used for experiments with the soot samples. An integration time of 200ms was used for these experiments. Similar to the case of Stellar Net, as described before, some of the spectra generated were false spectra with an extreme variation of relative peak intensities from majority of the spectra collected. These false spectra were discarded and an average of the rest of spectra was calculated to represent the composition of the sample as determined by MHCD-OES technique

B.2. MHCD Analyses of Soot Samples

Soot samples were generated by the combustion of six materials and pyrolysis of two materials that were approved for use aboard spacecraft, namely Polypropylene, Polyurethane, Kapton, Silicone rubber, Halar, Teflon. All observed atomic and diatomic species produced by micro-plasma analysis of the six soot samples, their excited state emission wavelengths and designated spectral transitions are tabulated in table B.2. 1. This information forms the basis of the analyses and interpretation of the emission spectra graphs.

Elemental species	Wavelength (nm)	Spectral Transitions
SiO^{31}	232	$(A^1\Pi\text{-}X^1\Sigma)$
Si^{31}	252	$(^3P^0\text{-}^3P)$
Si^{31}	288	$(^1P^0\text{-}^1D)$
CN^{44}	388	$(B^2\Sigma^+\text{-}X^2\Sigma^+)$
$CH(A\text{-}X)^{31}$	431	$(A^2\Delta\text{-}X^2\Pi)$
$C_2(D\text{-}X)^{45}$	231	$(D^1\Sigma_u^+\text{-}X^1\Sigma_g^+)$
C^{45}	247	$^1P^0\text{-}^1S$
$C_2(d\text{-}a)^{46}$	473	$d^3\Pi_g\text{-}a^3\Pi_a$
$C_2(d\text{-}a)^{46}$	516	$d^3\Pi_g\text{-}a^3\Pi_a$
$C_2(d\text{-}a)^{46}$	563	$d^3\Pi_g\text{-}a^3\Pi_a$
$H\text{-}\alpha^{31}$	656	3n-2n

Table B.2.1: Wavelength and spectral transition of the UV-Vis emission lines by MHCD analyses

All six soot spectra showed the diatomic emission band from the OH ($A^2\Sigma^+$-$X^2\Pi$) radical at 310 nm. The peaks at 337nm and 358nm are N_2($C^3\Pi_u$-$B^3\Pi_g$) emission bands which comes from the air contamination in the chamber. Also, a strong emission at 589 nm was detected in most of the soot spectra, identified as Na ($^2P^0$-^2S) the occurrence of which can be explained by the frequent use of sodium-containing compounds in polymer processing resulting in Na contamination.

I) Polypropylene:

Polypropylene is a very commonly used spacecraft material and has numerous applications in space exploration which include blending it with glass-fiber and using it for paneling[47]. Polypropylene, also known as polypropene, is a thermoplastic polymer having a molecular formula $(C3H6)_n$. It is made from the propylene monomer. Since polypropylene is composed of carbon and hydrogen, the spectrum obtained by the micro-plasma analysis of the soot sample mainly shows hydrogen present in the form H-α (656nm) and the different spectral forms of carbon. Spectral emissions bands of CH at 431nm and CN at 389 nm are observed whereas an atomic emission line of carbon appears at 248nm. The C_2 diatomic emission lines (the Swan band) are observed by emission from vibrational transitional progression of 2-0, 1-0 and 0-0 at 473, 516, and 563nm respectively. These emission lines (Swan band) are the result of incomplete molecular dissociation of C-C bonds. It arises as an intermediate of molecular breakdown.

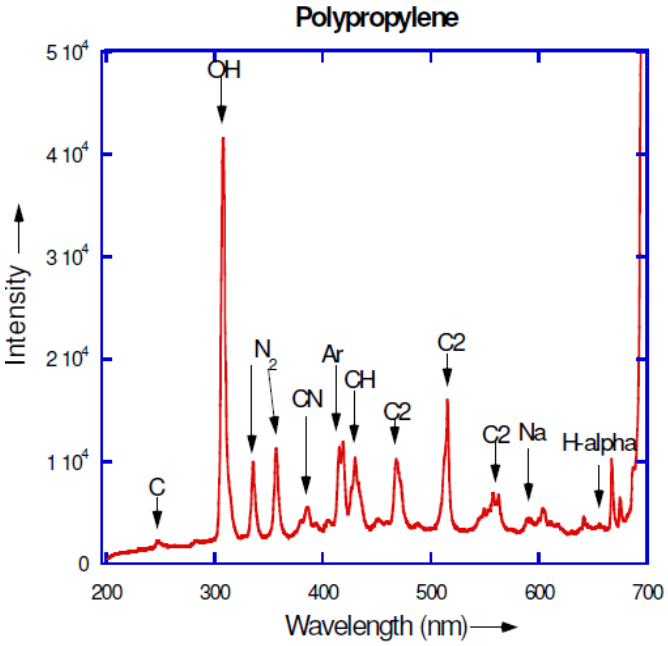

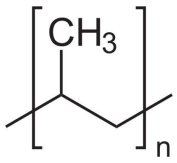

(a) (b)

Fig.B.2.1: a) Polypropylene soot spectrum b) Chemical structure of Polypropylene

II) Polyurethane:

Polyurethane foams are used to protect and insulate the external fuel tank of space shuttle[48]. It is a polymer composed of a chain of organic units joined by carbamate (urethane) links as shown in fig.B.2.2. Soot from polyurethane, like polypropylene soot, dissociates on plasma analysis to different species such as CH, CN, elemental carbon and also forms di-atomic carbon (C_2) bands such as the Swanband and Mullikan band. Contrary to the previous case, a high intensity CN peak is observed in this spectrum which represents the CN group from the polyurethane monomers. Moreover, in this case there exists a possibility of NH and NO radical formation, in the plasma, which upon

excitation emit wavelengths at 336nm and 358nm respectively. Thus these are also represented in the spectra along with N_2 which has emission lines at similar wavelengths[49].

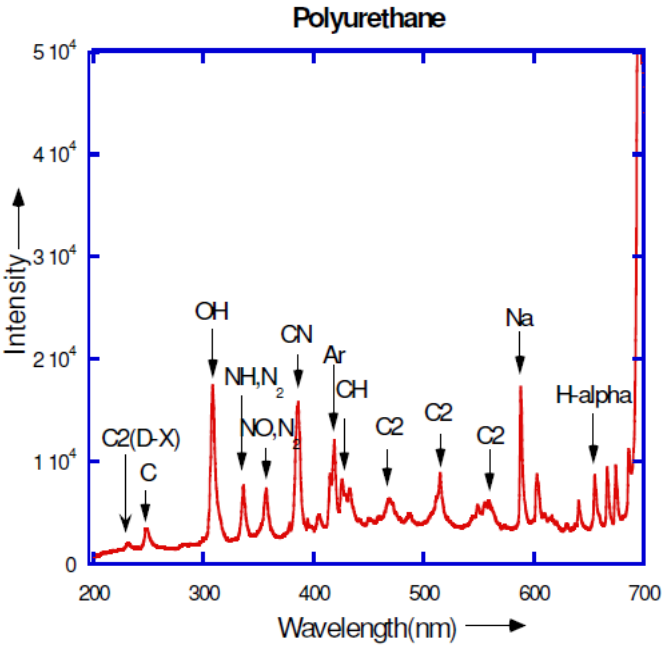

(a)

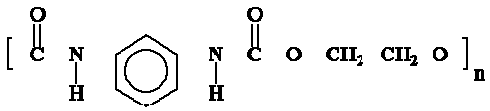

(b)

Fig. B.2.2: a) Polyurethane soot spectrum b) Chemical structure of Polyurethane

III) Kapton:

Kapton has widespread applications in space exploration. It is regularly used as an insulator in ultra-high vacuum environments due to its low outgassing rate. It finds application in flexible printed circuits and thermal micrometeoroid garments (the outside layer of space suits)[50]. It is also used as thermal insulation. Wires are coated with Kapton which acts as an insulator. Kapton can also be used as a good plastic support for solar

sails because of its durability in the space environment. Kapton, represented by the Chemical formula $(C_{22}H_{10}N_2O_5)_n$, has a cyano- group present in its base molecule which results in a high intensity CN peak in the spectra, obtained by MHCD-OES analysis of the Kapton soot. This differentiates it from other compounds which do not have nitrogen in the molecular formula. As like other soots Kapton soot also displays the spectral transitions of carbon in the form of Swan bands, Mullikan bands in addition to atomic carbon transitions and CH (A-X) radical emission.

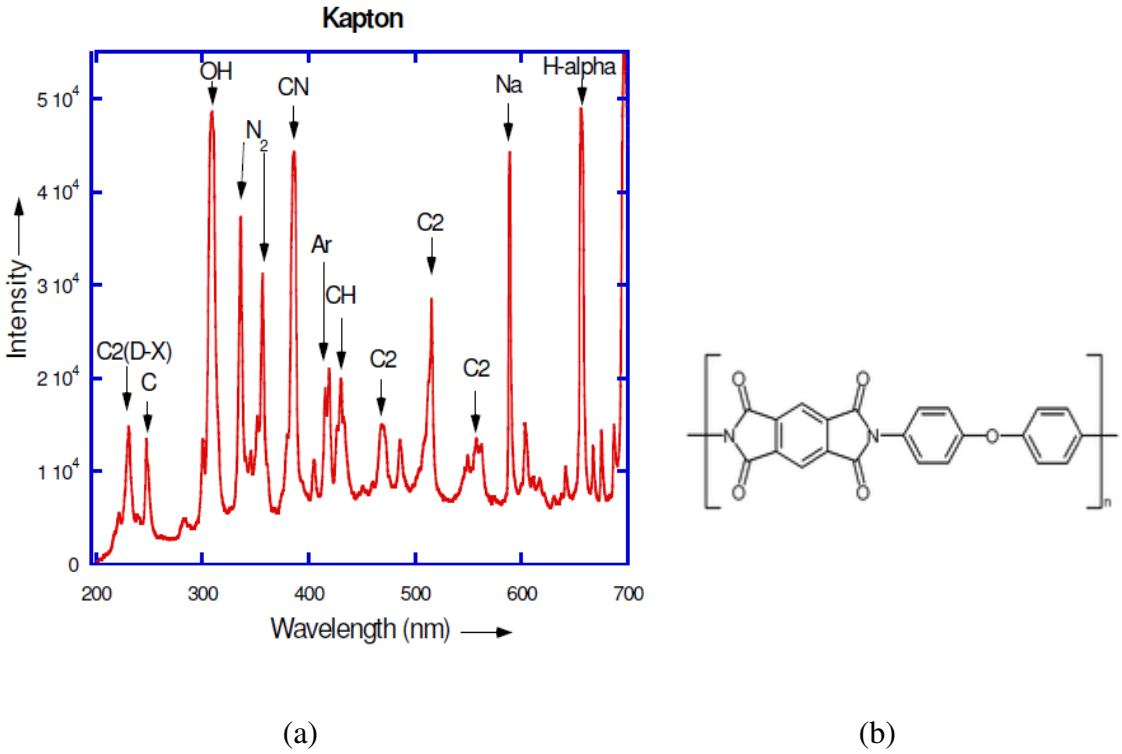

(a) (b)

Fig B.2.3: a) Kapton soot spectrum b) chemical structure of Kapton

IV) Silicone Rubber:

Silicone rubber is widely used in spacecraft because of its properties such as electrical insulation and resistance to radiation. It is used as a binder between the cover glass and solar cells as well as between the cells and base plate. It is also used as sealant[51]. Silicone rubber is composed of silicone ($[R_2SiO]_n$, where R is an organic group. The MHCD-OES analysis of Silicone rubber soot results in prominent emission lines of Si at 252nm and 288nm coming from Si present in the sample. Optical emission band of SiO is also observed at 232nm along with C_2 Mullikan band. Moreover the absence of a C-C bond in the molecule is reflected by the very low intensity peaks of C_2 and associated swan band emissions.

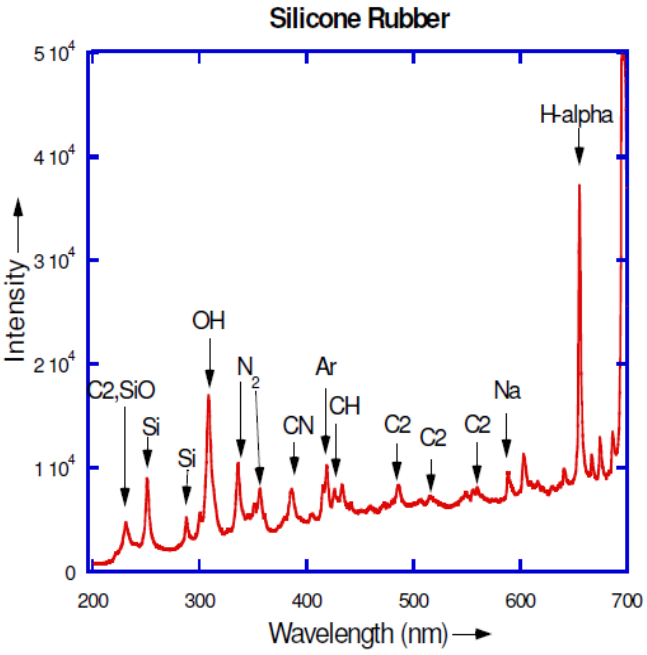

(a)

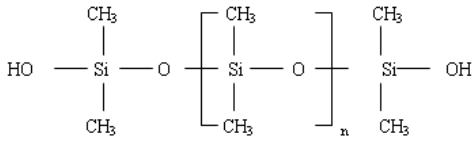

(b)

Fig B.2.4: a) MHCD-OES spectrum of Silicone Rubber soot b) Chemical structure of Silicone rubber

V) Halar:

Halar is used in aerospace for its high temperature, flame retardant properties and excellent chemical resistance. It is also used as insulator for wires in numerous spacecraft components[52]. Halar or ethylene chlorotrifluoroethylene is a copolymer of ethylene and chlorotrifluoroethylene. The fluorine and chlorine atoms present in halar form very stable compounds of HCl and HF during combustion. As a result, when the halar soot samples are analyzed later using MHCD technique, the elemental emission lines of F and Cl are not observed. Due to the presence of C-C bonds in the structure, the MHCD analysis of halar soot also produces C_2 emission bands such as the Carbon Swan Band and Carbon Mullikan band along with the emission lines of elemental carbon.

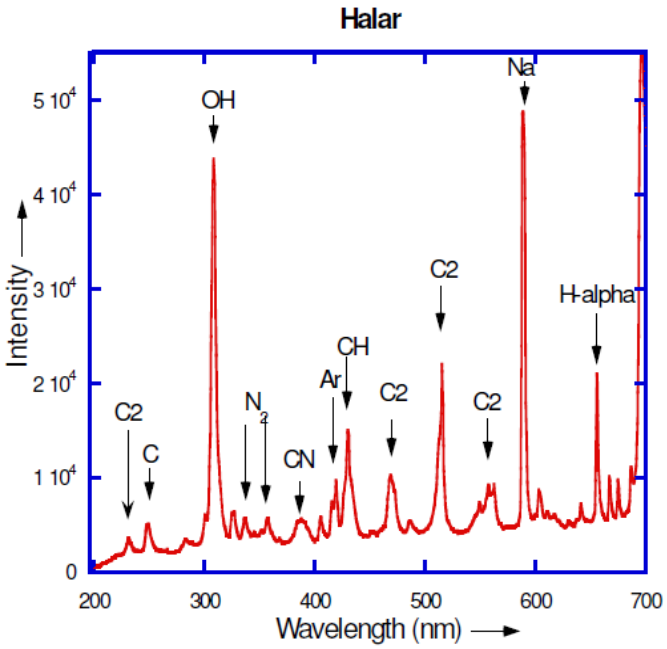

(a)

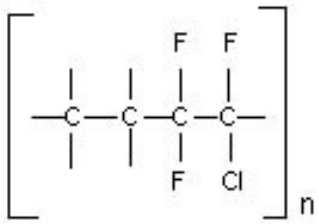

(b)

Fig.B.2.5: a) MHCD-OES Spectrum of halar soot b) Molecular structure of halar

VI) Teflon:

In this work, FEP brand (fluorinated ethylene propylene) of Teflon was tested. This type of Teflon is commonly used as a fabric for astronaut spacesuits[53]. Teflon or fluorinated ethylene propylene consists of Fluorine which on combustion forms Hydrogen Fluoride gas and escapes. Hence MHCD-OES analysis of Teflon soot does not yield any Fluorine peak. Moreover, Teflon does not have any CH units in its monomar which explains the absence of CH emission bands in the Teflon MHCD-OES spectrum. As hydrogen is also not present in the monomer, the H-α line observed is the result of optical emission from hydrogen in ambient moisture and consequently of low intensity.

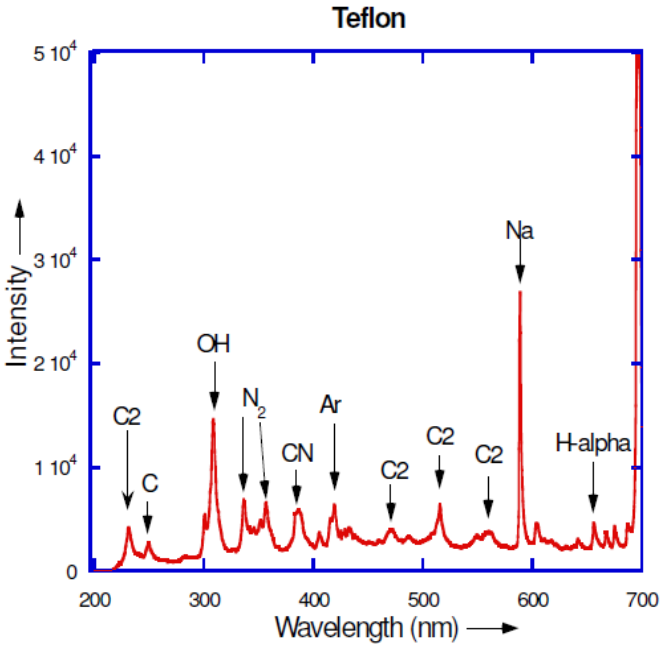

(a)

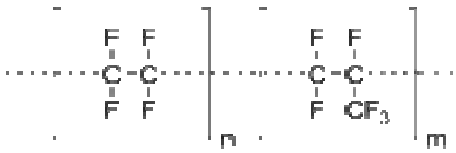

(b)

Fig B.2.6: Spectrum of Teflon soot and Molecular structure of Teflon

Fig.B.2.7 compares the MHCD-OES spectra of the six soot samples derived from six different compounds and therefore highlights the distinctiveness of each spectrum from the other.

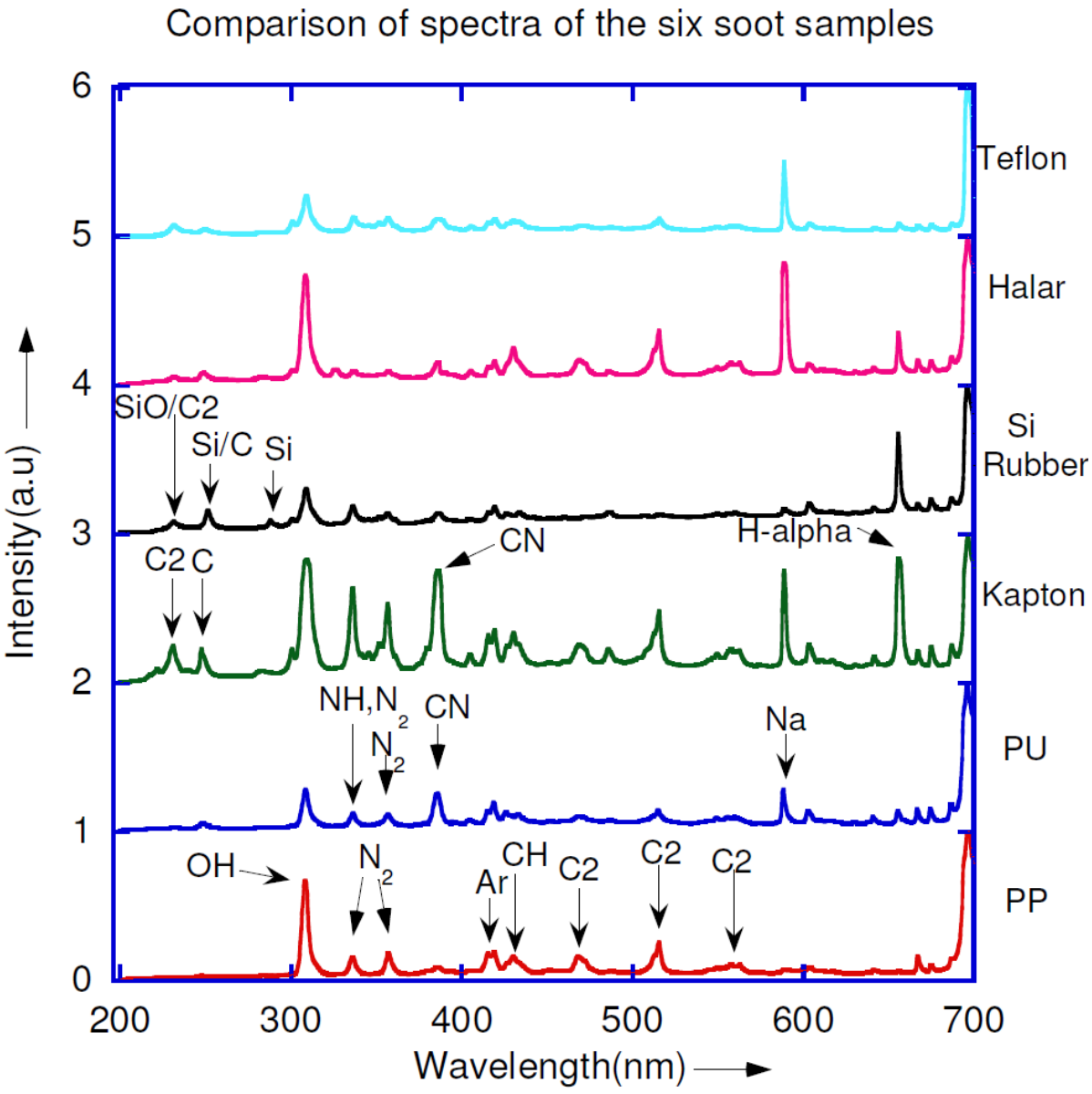

Fig B.2.7: Summary graph of the MHCD-OES Analyses of the six soot samples

All six soot spectra showed the diatomic emission band from the OH radical at 310 nm, a prime indicator of plasma induced reaction. The silicone rubber soot in particular shows the characteristic Si atomic lines at 252 and 288 nm and the excited SiO radical at 232 nm. The emission bands from excited CH radicals, at 387 and 431 nm and C2 (triplet Swan band systems) at 473, 516 and 563 nm are present in all soot samples. However the corresponding intensities of these bands are substantially different. In addition, depending on the soot sample, (and material or origin), the bands of N_2 at 337 and 358 nm,

CN at 388 nm and H_α at 656 nm show quite different intensities in the microplasma analytical spectrum. Polyurethane and Kapton soot spectra having CN units in their monomer show very strong spectral emission line of CN in their respective MHCD-OES spectra.

B.3. Analysis of the MHCD-OES spectra for distinctiveness

Since the line position, i.e. wavelength is a fingerprint of an element or diatomic specie, and that the intensities of the atomic lines and diatomic bands represents their concentrations, it is possible to identify the source (burning material) of the fire event by analyzing the soot's optical emission spectrum. Each soot sample produces a unique UV-VIS spectrum that is traceable to the particular burning material. In order to facilitate the visualization of the spectral differences associated with the soot samples, the most prominent lines and bands were selected and used to build a spectral bar graph (stick spectra) representation for the MHCD spectra from each soot sample. The intensities of

the peaks have been normalized. Examples of these bar graph representations for polypropylene and Kapton soots are shown in Figure B.3.1.

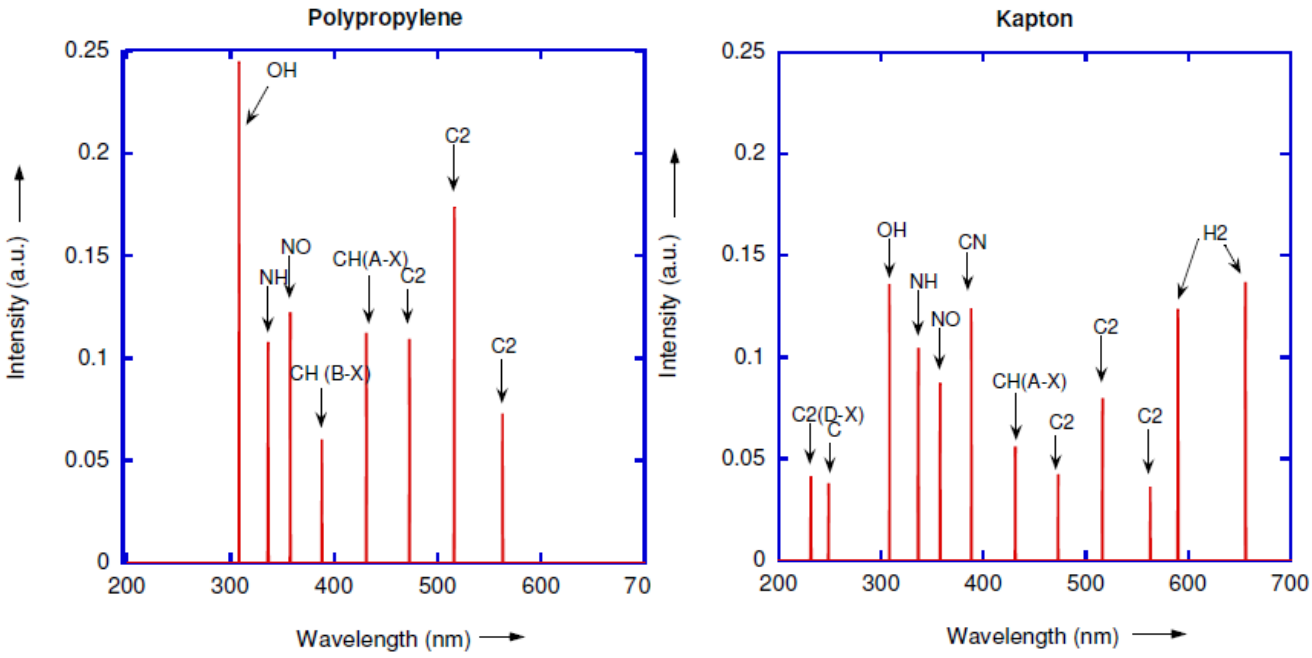

(a) (b)

Fig.B.3.1: Bar graphs representation of MHCD-OES spectra of (a) polypropylene and (b) Kapton soot.

The MHCD-OES spectra generated from the soot samples appeared characteristic to the respective tested materials and differed from each other. Such differences are the basis by which the MHCD could act as a 'smart' detector. With each spectrum unique to a specific material, comparison of an to the database would provide identification of the fire source. Such testing went beyond the tasks of this contract based work but would be a logical extension. To better illustrate the distinctiveness of the spectra, normalized stick spectra were calculated and plotted. As a set, to demonstrate their independence, residuals were

calculated. While such numbers lack reference comparison, the larger values suggest differentiation between this limited set of materials would be possible. Considering more materials as in a real vehicle a habitat may restrict such identification to classes of materials rather than specific ones. Still such variants would likely serve similar functions and be used in similar applications of locating fire source by identification of material class.

The basis for the 'smart fire sensor' is to be able to identify the soot forming material and therefore the source of fire. In order to illustrate the difference between different spectra, residuals were calculated by subtracting the two spectra bar graph representations. The binary spectral representations greatly simplified the mathematical operations towards distinguishing spectra. The residual difference can be expressed as:

$$d = I_{i1} - I_{i2}$$

where d = residual difference between two spectra

I_{i1}= Normalized intensity of the i^{th} emission line of soot spectra 1.

I_{i1}= Normalized intensity of the i^{th} emission line of soot spectra 2.

The residual differences should be zero if the spectra of the soot were alike (as they would be if arising from the same or even similar material). Fig.B.3.2 illustrates such residual differences between two MHCD-OES spectra. Produced by two different materials, the residual data differences were substantial in all cases, clearly illustrating the distinctiveness of the MHCD plasma analysis applied to soot of different origin.

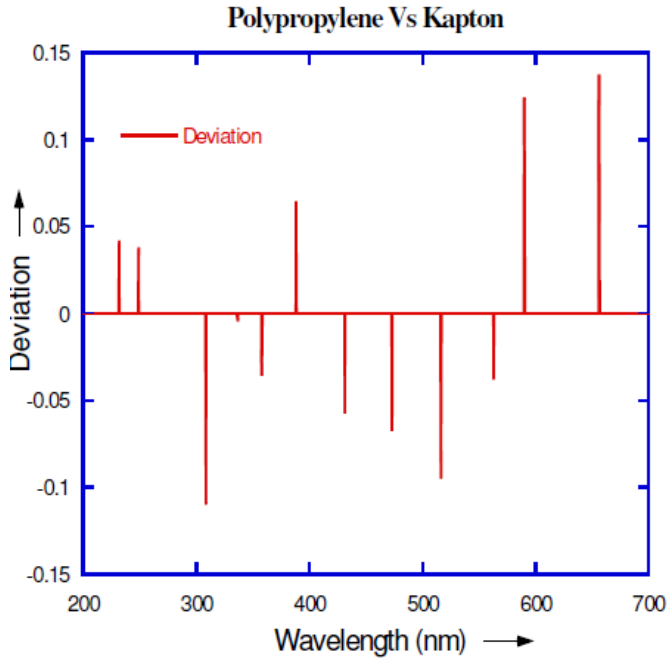
Polypropylene Vs Kapton
Deviation
Deviation
Wavelength (nm)
0.15
0.1
0.05
0
-0.05
-0.1
-0.15
200
300
400
500
600
700

(a)

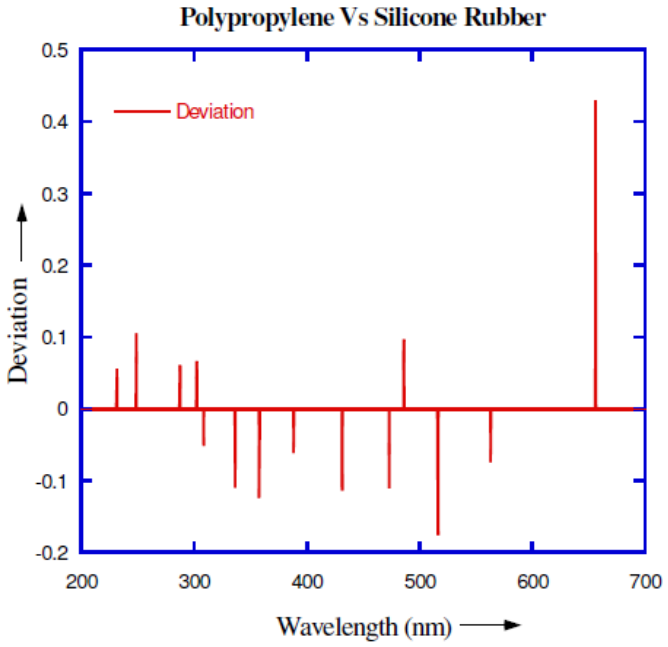
Polypropylene Vs Silicone Rubber
Deviation
Deviation
Wavelength (nm)
0.5
0.4
0.3
0.2
0.1
0
-0.1
-0.2
200
300
400
500
600
700

(b)

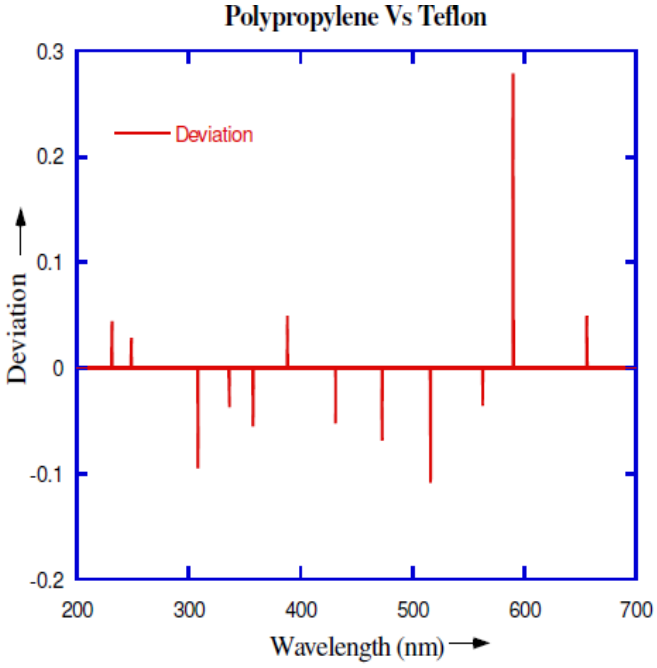
Polypropylene Vs Teflon
Deviation
Deviation
Wavelength (nm)
0.3
0.2
0.1
0
-0.1
-0.2
200
300
400
500
600
700

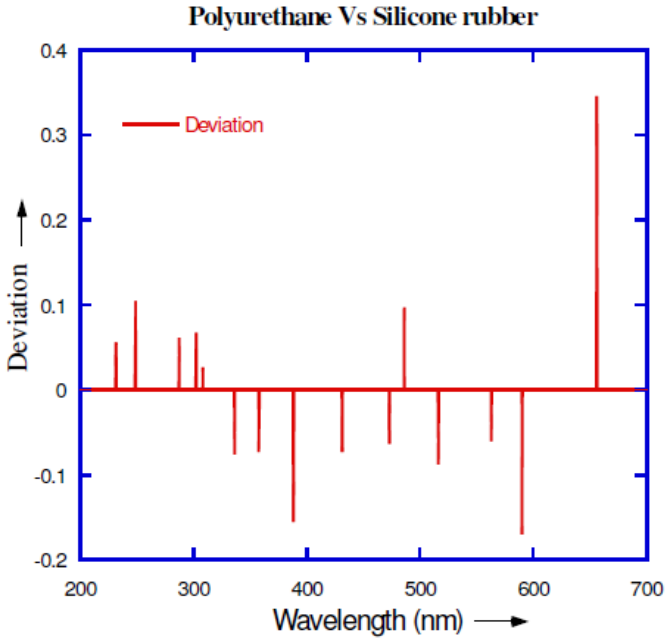
Polyurethane Vs Silicone rubber
Deviation
Deviation
Wavelength (nm)
0.4
0.3
0.2
0.1
0
-0.1
-0.2
200
300
400
500
600
700

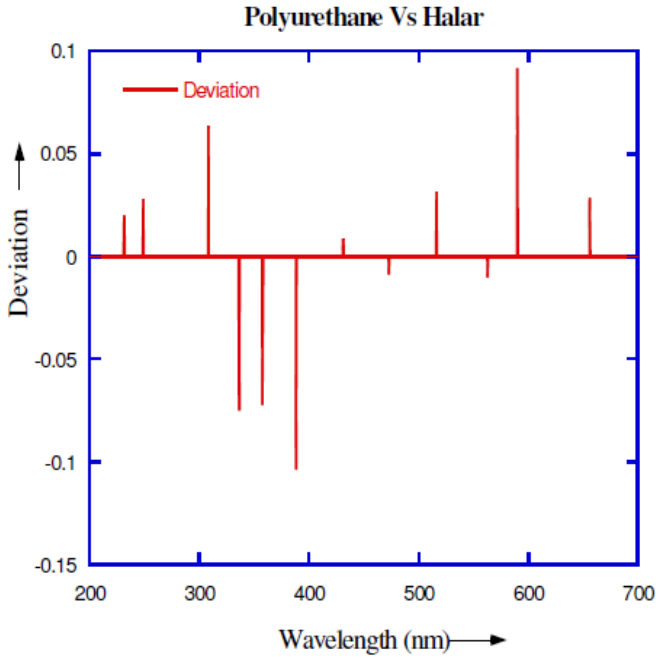
Polyurethane Vs Halar
Deviation
Deviation
Wavelength (nm)
0.1
0.05
0
-0.05
-0.1
-0.15
200
300
400
500
600
700

(e)

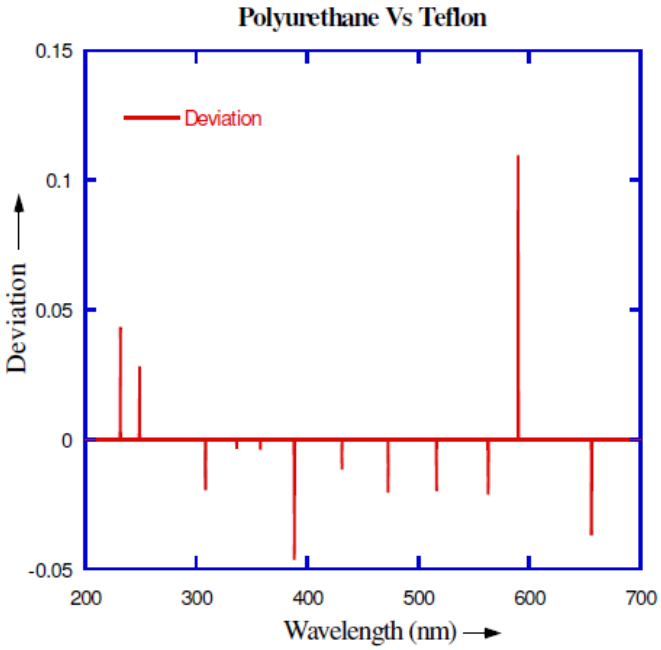
Polyurethane Vs Teflon
Deviation
Deviation
Wavelength (nm)
0.15
0.1
0.05
0
-0.05
200
300
400
500
600
700

(f)

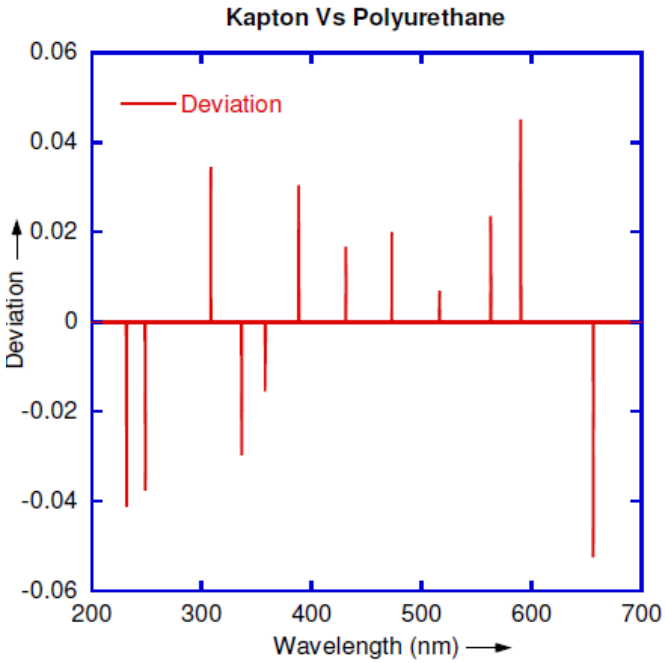
Kapton Vs Polyurethane
Deviation
Deviation
Wavelength (nm)
0.06
0.04
0.02
0
-0.02
-0.04
-0.06
200
300
400
500
600
700

(g)

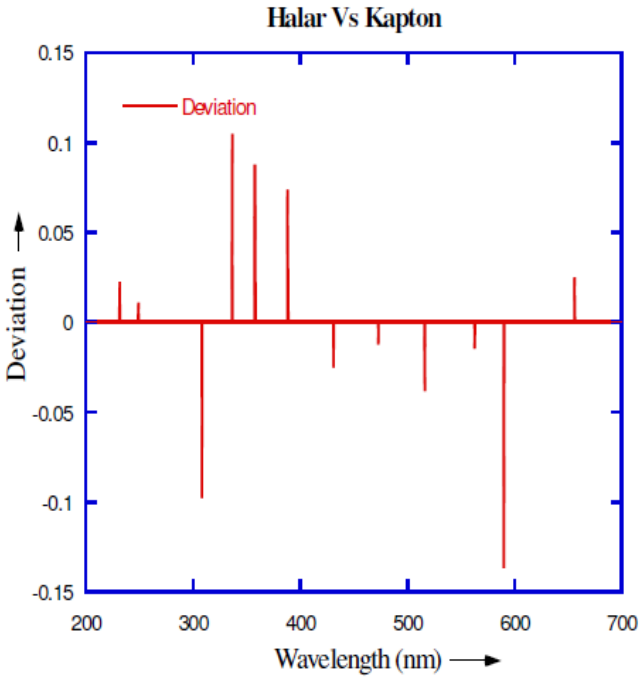
Halar Vs Kapton
Deviation
Deviation
Wavelength (nm)
0.15
0.1
0.05
0
-0.05
-0.1
-0.15
200
300
400
500
600
700

(h)

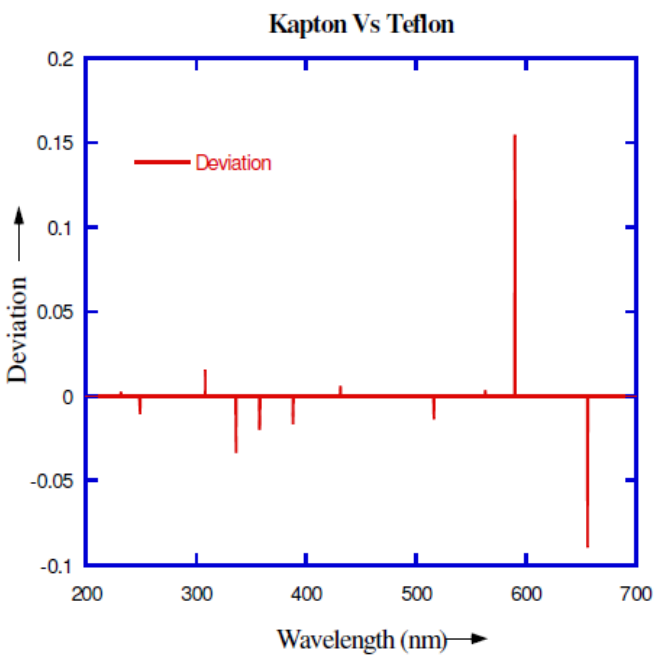
Kapton Vs Teflon
Deviation
Deviation
Wavelength (nm)
0.2
0.15
0.1
0.05
0
-0.05
-0.1
200
300
400
500
600
700

(i)

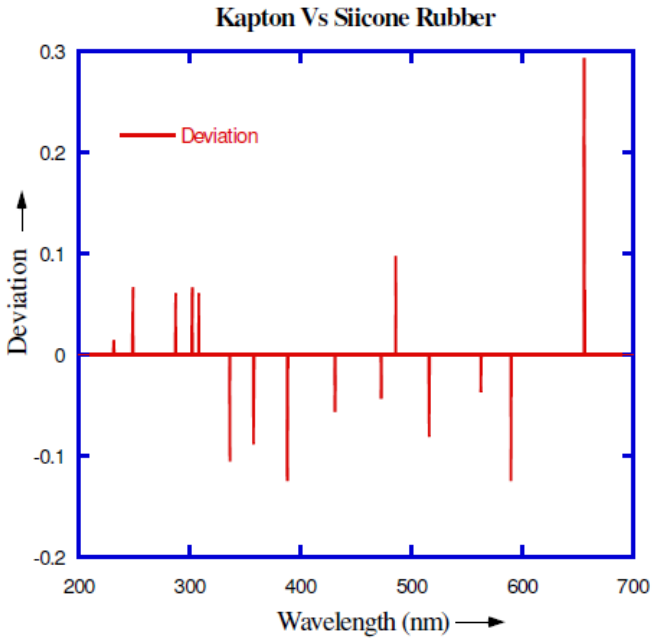
Kapton Vs Siicone Rubber
Deviation
Deviation
Wavelength (nm)
0.3
0.2
0.1
0
-0.1
-0.2
200
300
400
500
600
700

(j)

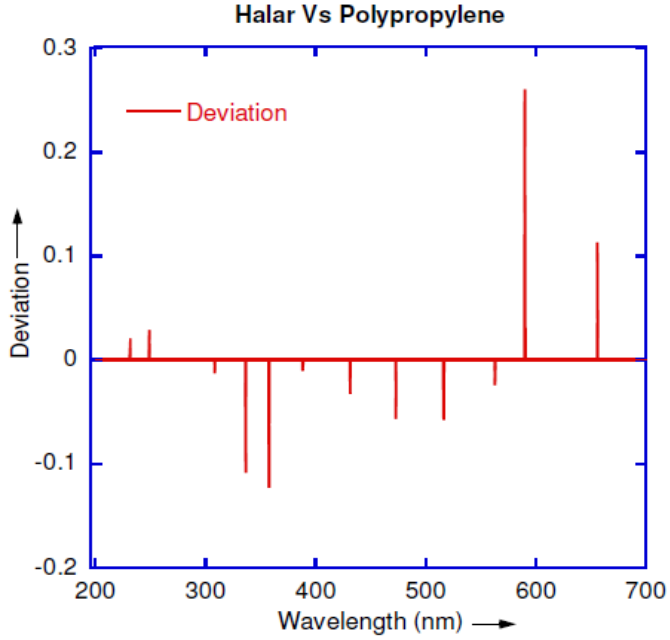
Halar Vs Polypropylene
Deviation
Deviation
Wavelength (nm)
0.3
0.2
0.1
0
-0.1
-0.2
200
300
400
500
600
700

(k)

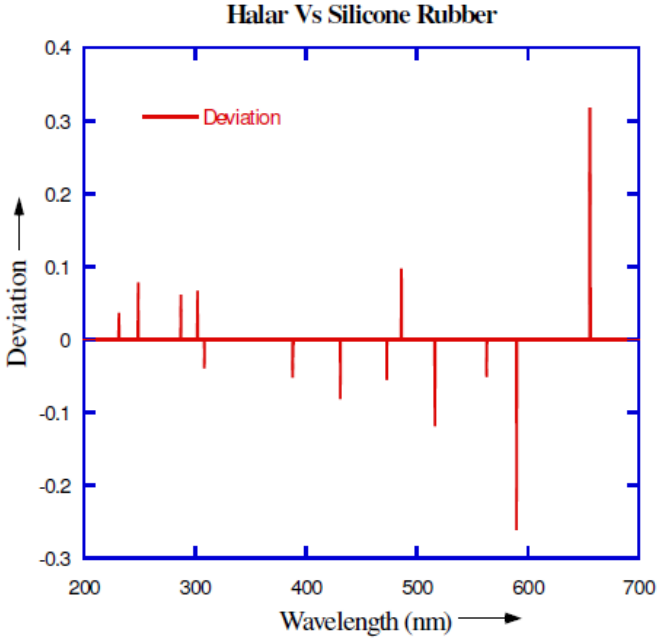
Halar Vs Silicone Rubber
Deviation
Deviation
Wavelength (nm)
0.4
0.3
0.2
0.1
0
-0.1
-0.2
-0.3
200
300
400
500
600
700

(l)

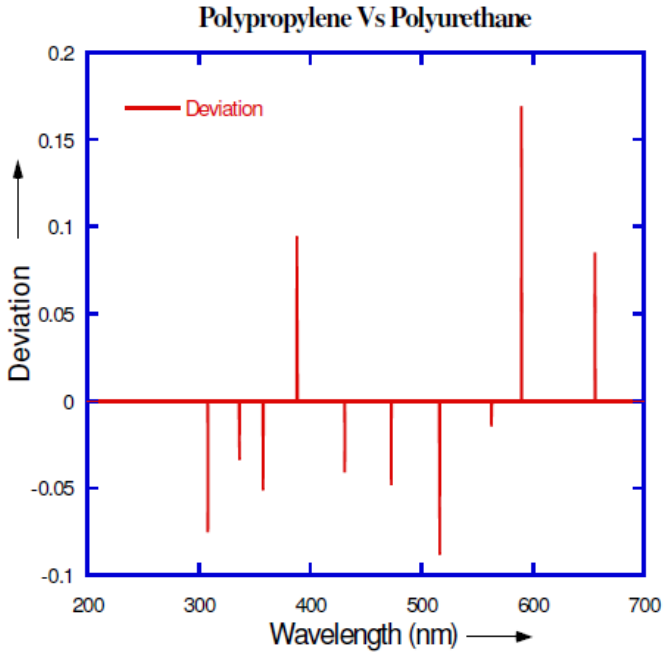

(m)

Fig B.3.2. Residual difference between spectral representations of the MHCD spectra of (a) Polypropylene-Kapton (b) Polypropylene-Silicone rubber (c)Polypropylene-Teflon (d) Polyurethane –Silicone rubber

(e) Polyurethane-Halar (f) Polyurethane-Teflon (g) Kapton –Polyurethane (h) Halar- Kapton (i) Kapton-Teflon (j) Kapton-Silicone rubber (k) Halar-Polypropylene (l)Halar –Silicone rubber(m)Polypropylene-Polyurethane

These normalized stick spectra of soot of materials commonly used in spacecraft can form the basis for a spectral database which would be of great value in present and future habitats and vehicles. The MHCD-OES analysis result of an unknown soot sample provides the fingerprint of the sample that can be matched against the database for its identification. Creating a data base would enable the MHCD-OES detector to be used for burning material identification which would be of a significant advancement in fire

detection and technology, which can then not only detect fire but also identify the source of fire.

B.4 C/H Ratio Calculation of Model Compounds

Figure.4.3.1. shows the emission spectra of three model compounds serving as different C/H standards: dodecane ($C_{12}H_{26}$), naphthalene ($C_{10}H_8$) and carbon black (amorphous carbon). These materials were analyzed by means of our atmospheric pressure MHCD plasma system. The elemental content of carbon and hydrogen for each sample is presented in Table 2.

The band at 516 nm (C2 Swanband) and the 656 nm line (H-α) was used to calculate the C/H ratio of the samples, as evidenced by the increase of H line intensity and decrease of C_2 band intensity moveing from the optical emission spectra of carbon black to naphthalene to dodecane, one observes an increase of the H-line intensities and decrease of the C_2 band intensity. This can be clearly observed by means of Table 2 which tabulates the relative decrease in C-atom and increase in H-atom content across these reference compounds. For comparison, two carbonaceous aerosols evolved from the pyrolysis of polypropylene at 500 and 900 ^{o}C were included in Figure 7 and Table 2. All the data were normalized using the 697 nm argon spectral line as a peak reference (given a reference value = 1).

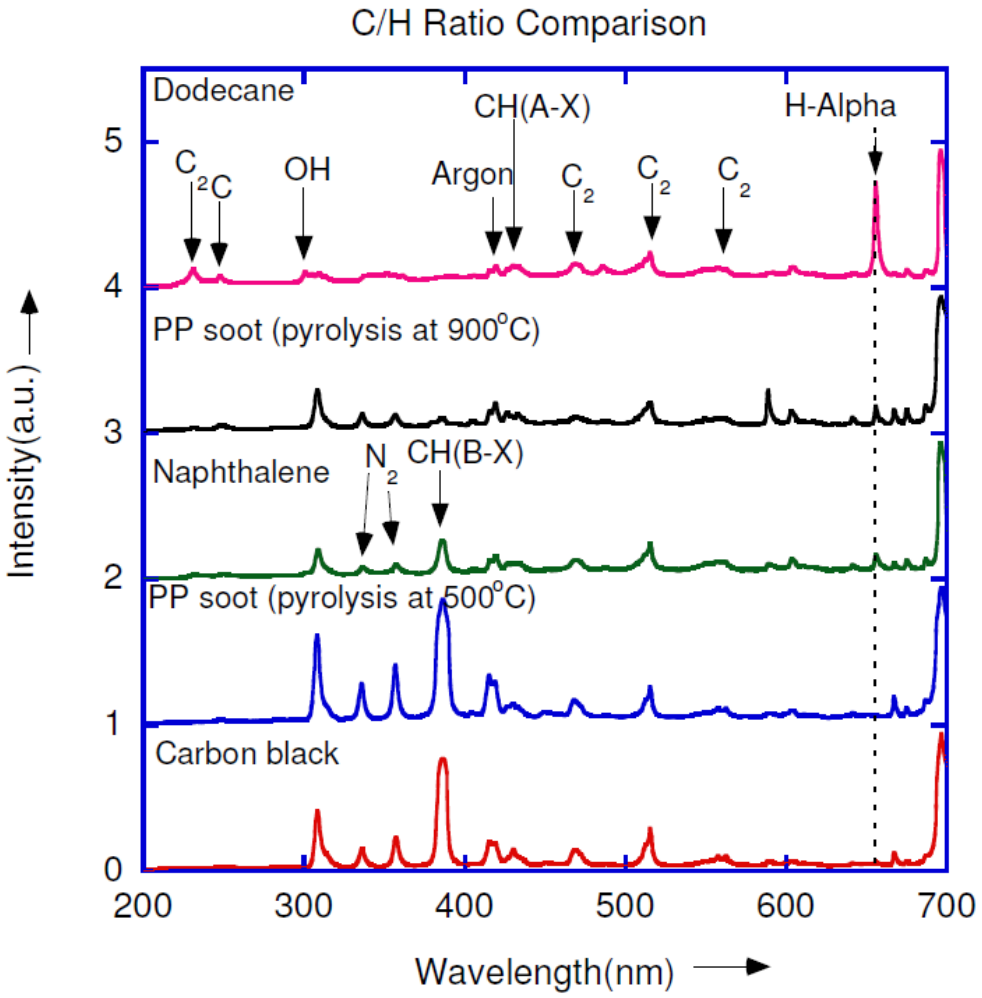

Fig.B.4.1: Optical emission spectra of the model C/H ratio standards along with pyrolysis products of Polypropylene at 500 °C. and 900 °C.

Based on the results of the intensity ratio between C2 band (516 nm) and H-atom line (656 nm), the evolved particulates from pyrolysis of PP at 500 °C have an atomic C/H ratio similar to naphthalene. It has been observed that at this temperature, the particulates were a mixture of carbon soot and condensable (medium to high molecular weight

hydrocarbons), i.e., the products from the partial carbonization and depolymerization processes respectively. At 900 ^{o}C, it was expected that the depolymerization with much more carbonization would be attained, resulting in increasing the conversion of PP into elemental carbon soot. As a result, the atomic C/H ratio should increase as function of the pyrolysis temperature. It may be observed from Table B.4.1 that intensity ratio between C2 band and H-atom line for the pyrolytic soot of PP obtained at 900 ^{o}C has a value close to carbon black, *confirming the projected composition change*.

Compound	C (%)	H (%)	Atomic ratio C/H	Intensity of C2 band (516nm)	Intensity of H line (656nm)	C2 band Int. /H line Int.
Carbon Black	78.36	20.22	3.87	22538	7785	2.89
PP soot (900^{o}C)	NA	NA	NA	21344	8599	2.48
Naphthalene	55.56	44.44	1.25	17160	13442	1.28
PP soot (500^{o}C)	NA	NA	NA	16160	14440	1.12
Dodecane	31.57	68.43	0.46	16796	43988	0.38

Table B.4.1. Comparison of the C/H ratio obtained from elemental composition and from spectra analysis

The quasi-linear correlation between the real atomic C/H ratios of the standards (dodecane, naphthalene and carbon black) and the C/H results of same samples obtained with the newly developed spectroscopic technique can be seen in Figure B.4.2. It has a

correlation coefficient of .981. This highlights the analytical potential of the MHCD detector for analysis of carbonaceous particulates by the C/H ratio.

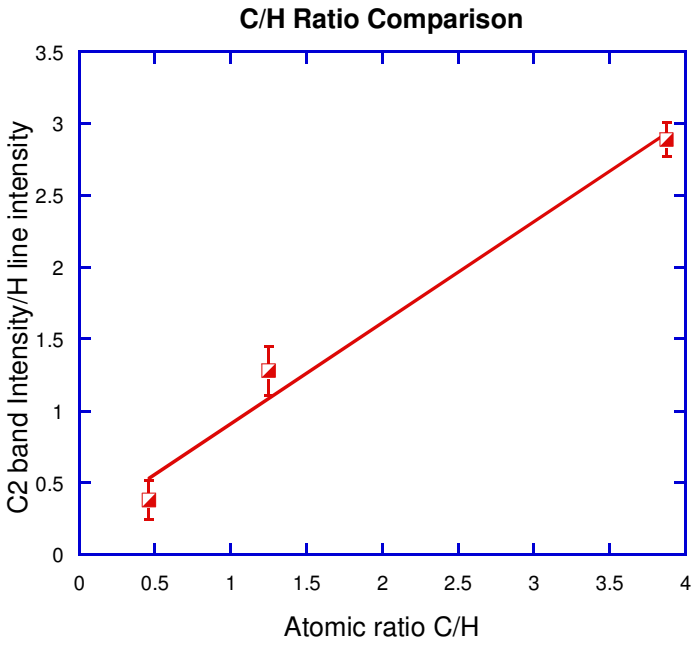

Fig: B.4.2: Correlation between actual C/H ratio and that obtained using micro-plasma device

B.5. Inorganic Materials

In current spacecraft, automated early warning of fire events is achieved through smoke detectors, using principles of light scattering or ionization-current detection. However, the effectiveness of these detectors that were initially designed to work in a normal gravity environment has been contested because the potential fire-causing accidents that have occurred in the Space Shuttle were identified by the crewmembers, rather than the fire detectors.

Both detection methods reported above are not specific to the main degradation products of a fire event. The main degradation products from materials are light gases, semi-volatiles and particulates. Dust and other inorganic impurities such as salts from human transpiration can be detected by the fire sensors and erroneously induce a fire alarm.

To test the ability of the MHCD to differentiate between the soot samples and inorganic samples, MHCD-OES spectra of some model inorganic compounds were recorded. Figure B.5.1 compares the spectra of different inorganic materials, sodium chloride, ammonium sulfate, silica and alumina. For comparison, a soot sample, generated from the combustion of polypropylene is included for comparison. The inorganic samples show their characteristic emission lines e.g NaCl shows the emission line of Na at 589nm, silica shows the characteristic emission bands of atomic Si at 252 and 288nm and SiO band at 288nm, Alumina shows Al emission lines at 393nm etc.

Across all the samples, the soot MHCD-OES spectra across all samples show the characteristic CH (431 nm) and C2 Swanband (473, 516, 563 nm) emissions. These atomic and diatomic spectral bands are not observed in the emission spectra of inorganic samples. This confirms that the MHCD-OES detector is highly specific to materials and can be specific to carbon (soot) to avoid false positive events.

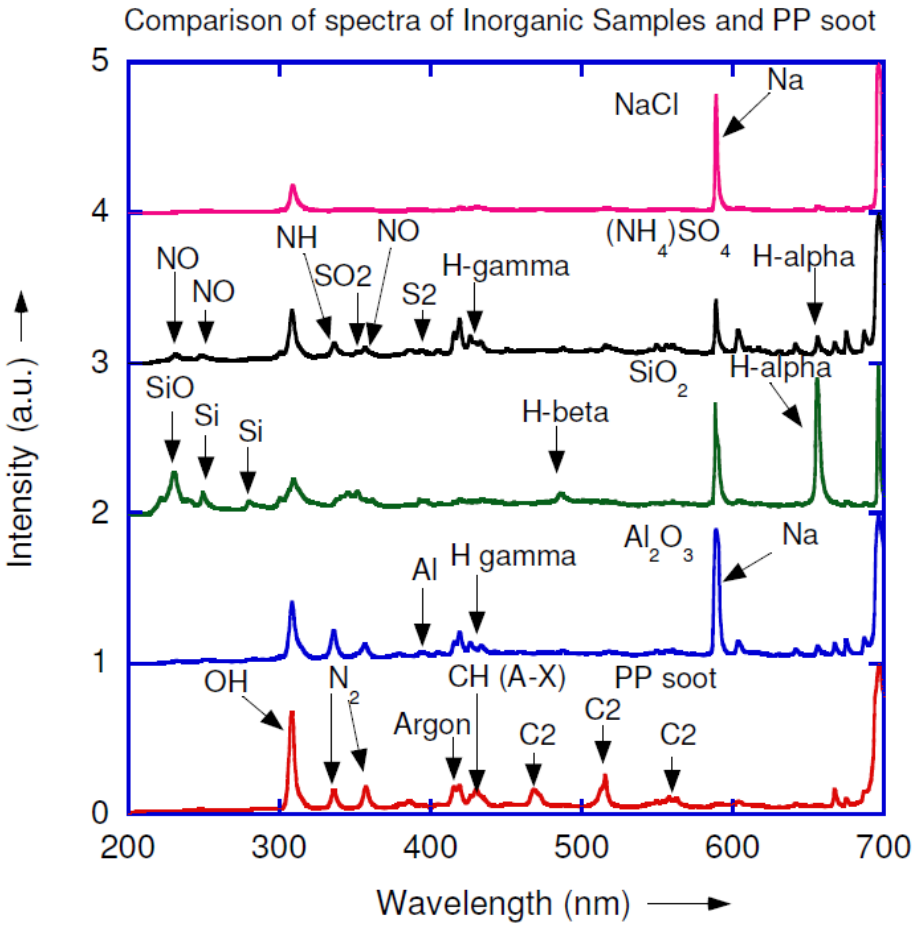

Fig.B.5.1: Comparison of inorganic sample soot spectra with fire-safety (organic) soot spectra

B.6 Summary:

The results illustrated in this chapter demonstrate that the micro-hollow glow discharge plasma-based analysis system is capable of detecting and identifying combustion produced soot to its source. Based upon the distinctiveness of the MHCD plasma spectra, the (material) source of the fire event can be identified by analyzing the MHCD plasma emission spectrum of the corresponding soot.

The micro-plasma analysis method is also able to determine the C/H elemental ratio of carbonaceous aerosols and distinguish these combustion-produced emissions from ambient inorganic (nuisance) aerosols. The MHCD emission spectra of carbonaceous particles show characteristic spectral emission atomic lines and diatomic bands that are absent in the spectra of inorganic samples. This confirms that the micro-plasma detector is highly specific to smoldering or combustion events (by selective detection of emission products) and can reduce if not eliminate false alarms due to ambient dust and detritus. Reciprocally, the MHCD can serve a dual function of environmental monitoring for astronaut health by yet detecting and quantifying such inorganic aerosols.